



# Modeling Studies of Chromatin Fiber Structure as a Function of DNA Linker Length

Ognjen Perišić<sup>1†</sup>, Rosana Colleparado-Guevara<sup>1†</sup> and Tamar Schlick<sup>1,2\*</sup>

<sup>1</sup>Department of Chemistry, New York University, 100 Washington Square East, New York, NY 10003, USA

<sup>2</sup>Courant Institute of Mathematical Sciences, New York University, 251 Mercer Street, New York, NY 10012, USA

Received 3 November 2009;

received in revised form

24 July 2010;

accepted 29 July 2010

Edited by D. Case

## Keywords:

chromatin;

mesoscale modeling;

linker histone;

fiber condensation

Chromatin fibers encountered in various species and tissues are characterized by different nucleosome repeat lengths (NRLs) of the linker DNA connecting the nucleosomes. While single cellular organisms and rapidly growing cells with high protein production have short NRL ranging from 160 to 189 bp, mature cells usually have longer NRLs ranging between 190 and 220 bp. Recently, various experimental studies have examined the effect of NRL on the internal organization of chromatin fiber. Here, we investigate by mesoscale modeling of oligonucleosomes the folding patterns for different NRL, with and without linker histone (LH), under typical monovalent salt conditions using both one-start solenoid and two-start zigzag starting configurations. We find that short to medium NRL chromatin fibers (173 to 209 bp) with LH condense into irregular zigzag structures and that solenoid-like features are viable only for longer NRLs (226 bp). We suggest that medium NRLs are more advantageous for packing and various levels of chromatin compaction throughout the cell cycle than their shortest and longest brethren; the former (short NRLs) fold into narrow fibers, while the latter (long NRLs) arrays do not easily lead to high packing ratios due to possible linker DNA bending. Moreover, we show that the LH has a small effect on the condensation of short-NRL arrays but has an important condensation effect on medium-NRL arrays, which have linker lengths similar to the LH lengths. Finally, we suggest that the medium-NRL species, with densely packed fiber arrangements, may be advantageous for epigenetic control because their histone tail modifications can have a greater effect compared to other fibers due to their more extensive nucleosome interaction network.

© 2010 Elsevier Ltd. All rights reserved.

## Introduction

The genome of every living organism contains the complete information and guidelines required for

the organism's growth and development. Intriguingly, the DNA storage and manipulation mechanisms have to satisfy two antagonistic requirements: a high compaction ratio and facile access to the genome. Understanding how the internal organization of DNA achieves both factors is crucial for our understanding of the most basic cellular processes.

DNA storage in eukaryotic cells is achieved through the chromatin fiber. The basic chromatin building block is the nucleosome: a histone core composed of four pairs of protein dimers (histone proteins H2A, H2B, H3, and H4) around which 147 bp of DNA are wound 1.75 turns.<sup>1</sup> Every histone dimer has two protruding tails (H2A has four),

\*Corresponding author. Department of Chemistry, New York University, 100 Washington Square East, New York, NY 10003, USA. E-mail address: [schlick@nyu.edu](mailto:schlick@nyu.edu).

† O.P. and R.C.-G. contributed equally to this work.

Abbreviations used: NRL, nucleosome repeat length; LH, linker histone; MC, Monte Carlo; ES, embryonic stem; EM, electron microscopy; DiSCO, discrete charge optimization; PBE, Poisson–Boltzmann equation.

63 which are highly positively charged and thus  
64 readily available for interactions with the DNA  
65 polyelectrolyte.

66 The length of the DNA wrapped around the  
67 nucleosome core (147 bp) plus the length of the  
68 DNA linker (or 'linker' for short therein) connecting  
69 each nucleosome to the next [nucleosome repeat  
70 length (NRL)] varies within and between organisms  
71 (see Table 1).<sup>2,3</sup> While some simple organisms have  
72 short DNA linkers ranging from 18 to 45 bp, the  
73 typical DNA linker length for mature, transcriptionally  
74 inactive eukaryotic cells, between 50 and 60 bp,  
75 leads to NRL values between 197 and 207 bp. Table  
76 1 shows that rapidly growing cells with high protein  
77 production are associated with a relatively short  
78 NRL ranging from ~160 to 189 bp; these include  
79 unicellular organisms, embryonic stem (ES) cells,  
80 and tumor cells. Mature cells tend to have longer  
81 NRL ranging between 190 and 220 bp. An exception  
82 to this trend is NRL in rat neurons, which is long  
83 before birth, 200 bp, and drops to 170 bp and less  
84 later on.<sup>4</sup> Longer NRL chromatin (220 bp) appears in  
85 starfish,<sup>3</sup> which resides in higher salt environments.

86 Monovalent ( $K^+$ ,  $Na^+$ ) and divalent ( $Mg^{2+}$ ) ions,  
87 as well as linker histone (LH) proteins H1/H5, are  
88 essential for chromatin fiber compaction.<sup>3</sup> Chromatin  
89 depleted of H1 is decondensed, with a decreased  
90 sedimentation velocity.<sup>5</sup> At low ionic strengths, this  
91 leads to a more open and randomly organized,  
92 beads-on-a-string form of the chromatin fiber.<sup>6-8</sup>

93 Spadafora *et al.* showed that the lack of H1 in the  
94 presence of highly concentrated monovalent ions  
95 (0.6 M) is associated with chromatin with very  
96 short NRL.<sup>9</sup> Recent experimental data also show a  
97 strong linear relationship between the number of  
98 LHs H1 per nucleosome and NRL.<sup>3</sup> H1 in living  
99 cells binds dynamically to both euchromatin and  
100 heterochromatin, in a 'stop-and-go' mode,<sup>10</sup> and  
101 switches its carrier nucleosome every several  
102 minutes.<sup>11</sup> Low H1 stoichiometry and short NRL  
103 also characterize newly replicated eukaryotic HeLa  
104 cells (NRL=165 bp).<sup>12</sup> H1 concentrations and NRL  
105 values in those cells rapidly evolve to the values  
106 present in mature chromatin.<sup>13</sup> The same behavior  
107 was observed in Ehrlich ascites tumor cells,<sup>14</sup>  
108 suggesting a relationship between these factors and  
109 certain tumors.

110 The detailed structure of the chromatin fiber has  
111 been a puzzle for more than three decades.<sup>15,16</sup> Early  
112 on, the first proposed structure for the 30-nm  
113 chromatin fiber was a one-start helix (solenoid)  
114 where every nucleosome is in contact with its  
115 immediate neighbors,  $i \pm 1$ .<sup>6,17</sup> The DNA linkers in  
116 this model are bent in the fiber interior. Such linker  
117 bending offers a relatively constant fiber width for  
118 different NRLs and can easily produce a 30-nm fiber  
119 with a packing ratio of 6 to 8 nucleosomes per 11 nm  
120 of fiber length. However, in this solenoid model, the  
121 role of LH is not clarified because the wide angle

**Table 1.** NRL within and between organisms

Species/tissue	NRL	t1.2
<i>Aspergillus nidulans</i> <sup>111</sup>	154	t1.4
Rat neuron <sup>112</sup>	162	t1.5
<i>Saccharomyces cerevisiae</i> <sup>113</sup>	165	t1.6
<i>Neurospora crassa</i> <sup>114</sup>	170	t1.7
H1c, H1d, H1e null ES <sup>115</sup>	174	t1.8
Amoebae <sup>116</sup>	176	t1.9
Chinese hamster ovary cells <sup>2</sup>	178	t1.10
Plasmodia <sup>116</sup>	181	t1.11
HeLa cells <sup>2</sup>	188	t1.12
Hepatoma cells <sup>2</sup>	188	t1.13
Teratoma cells <sup>2</sup>	188	t1.14
P815 cells (mouse mastocytes) <sup>2</sup>	188	t1.15
Myoblast cells <sup>2</sup>	189	t1.16
CV1 cells (African green monkey) <sup>2</sup>	189	t1.17
Wild-type mouse ES cells <sup>115</sup>	189	t1.18
H1 <sup>0</sup> , H1c, H1e null mouse thymus <sup>115</sup>	189	t1.19
BHK (Syrian hamster kidney) <sup>2</sup>	190	t1.20
Rat kidney primary culture <sup>2</sup>	191	t1.21
H1 <sup>0</sup> , H1c, H1e null mouse liver <sup>115</sup>	191	t1.22
Rat bone marrow <sup>2</sup>	192	t1.23
Rat fetal liver (14 days) <sup>2</sup>	193	t1.24
Wild-type mouse liver <sup>115</sup>	195	t1.25
Wild-type mouse thymus <sup>115</sup>	196	t1.26
Rat liver <sup>2</sup>	196	t1.27
Rat kidney <sup>2</sup>	196	t1.28
Syrian hamster liver <sup>2</sup>	196	t1.29
Syrian hamster kidney <sup>2</sup>	196	t1.30
Chick oviduct <sup>2</sup>	196	t1.31
Rat glia <sup>112</sup>	201	t1.32
Chicken erythrocyte <sup>117</sup>	212	t1.33
<i>Echinoderm sperm</i> <sup>3</sup>	~220	t1.34

122 between the bent linkers of entering and exiting  
123 nucleosomes generally excludes close interactions  
124 with the LH, though interactions between LH and  
125 non-parental DNA linkers are possible.

126 The second major type of proposed model for the  
127 30-nm chromatin fiber is a two-start helix (zigzag  
128 structure) in which straight DNA linkers crisscross  
129 the fiber axis and thus promote  $i \pm 2$  interactions  
130 between nucleosomes.<sup>18-22</sup> The straight linkers  
131 make the width of zigzag fiber model more strongly  
132 dependent on the NRL. In addition, the LH in this  
133 model has a clearly defined role, to attract the DNA  
134 linkers exiting/entering the parent nucleosomes and  
135 form rigid stems.<sup>7</sup>

136 Since 1980, many studies have supported aspects  
137 of both models. The early results by Williams *et al.*  
138 based on electron micrographs supported the two-  
139 start cross-linker model.<sup>19</sup> Their measurements  
140 indicated a strong linear relationship between the  
141 linker length and the fiber width for both *Necturus*,  
142 where the DNA linker length is 48 bp and fiber  
143 width is 31 nm, and *Thyone*, with a DNA linker  
144 length of 87 bp and a fiber width of 39 nm, in a  
145 buffer with monovalent and divalent ions. Later, the  
146 same group produced similar results using cryo-  
147 electron microscopy (EM) imaging.<sup>20</sup> They also  
148 showed that highly compacted chromatin fiber has  
149 solid centers,<sup>23</sup> which supported the idea that DNA  
150 linkers cross the fiber axis.

Electron tomography<sup>21</sup> showed that chromatin fibers under moderate salt concentration (0.15 M NaCl) have asymmetric zigzag structures determined by the properties of the nucleosome-linker unit. Irregularity in fiber structure is supported by many modeling studies.<sup>24–26</sup>

The correlated breaks in DNA produced by ionizing radiation offer an indirect way to view arrangements of nucleosomes.<sup>27</sup> The end-labeled fragments induced by correlated breaks and separated by gel electrophoresis exhibited characteristic peaks at 78 bp (one helical turn around histone core) and between 175 and 450 bp; these values reflect the positions of nearest neighbor nucleosomes and suggest a zigzag organization for chromatin.

The influence of LH on chromatin structure in higher eukaryotes was investigated by Bednar *et al.*<sup>7</sup> They showed that LH leads to the formation of a zigzag-promoting stem motif by mediating the close contact of the exiting and entering linker DNA. More recently, EM imaging combined with sedimentation coefficient measurements by Routh *et al.* demonstrated that short-NRL (167 bp) arrays form narrow fibers (21 nm diameter) in the presence of LH.<sup>28</sup> For medium-NRL arrays (197 bp), highly compact 30-nm fibers result.

Later, X-ray crystallography made an important contribution to the high-resolution nucleosome structures,<sup>1,29</sup> by producing a low-resolution image of a cross-linked tetranucleosome,<sup>22,30</sup> which supported a two-start zigzag. However, that structure was based on a fiber with short linkers (20 bp) and without LH.

The structure of chromatin has also been probed by disulfide bridging.<sup>31</sup> In such experiments, H2A/H2B and H4 histones are targets for cysteine replacement because their tail bases are crucial for compaction via interaction with H2A/H2B tails of neighboring nucleosomes.<sup>1</sup> Following endonuclease cleavage, the initial 10 to 12 nucleosome fibers were reduced to 5 to 6 nucleosome constructs that constitute the individual starts of the two-start configurations. This result was interpreted as evidence for zigzag configurations because one-start solenoids would preserve the initial connectivity ( $i \pm 1$  contacts) and retain the 12-nucleosome repeat pattern.

Initially, the one-start helical structure also had its proponents,<sup>6,32–35</sup> and recent results by Rhodes *et al.* have renewed this view.<sup>28,36–39</sup> These results suggest that for longer NRL with  $Mg^{2+}$  and LH, chromatin folds into an interdigitated one-start helix. The studies show that the chromatin fiber has a fairly constant diameter of 33–35 nm for moderate-length linkers (NRL between 177 and 207 bp) and 44 nm for long linkers (NRL between 217 to 237 bp). The moderate to long NRL fibers they analyzed have a high packing ratio, indicative of solenoid-like topology: 11 nucleosomes per 11 nm

for moderate-length linkers and 15 to 17 nucleosomes for long-linker arrays.<sup>28,37</sup> However, for short NRL (167 bp), their experiments<sup>28,39</sup> indicate that chromatin adopts a two-start helical arrangement with less compact (6.1 nucleosomes per 11 nm) and thinner (21 nm diameter) fibers.

Recent computational studies using a coarse-grained model described by several tunable parameters such as the linker DNA opening angle and twisting angle between successive nucleosomes<sup>25</sup> found periodic patterns in fiber dimensions for NRL from 202 to 222 bp, a strong effect of NRL on the viable chromatin conformations (two-start and three-start were found), and increased structural irregularity for  $NRL > 214$  bp. While such patterns agree with X-ray scattering studies,<sup>19</sup> they differ from the above-cited work.<sup>37</sup> Modeling based on EM measurements of reconstituted fibers, however, show a range of possible conformations as NRL changes,<sup>26</sup> the authors emphasize ‘the multiplicity of fiber structures!’ tuned by the NRL. Moreover, Monte Carlo (MC) simulations of coarse-grained models of chromatin with NRL ranging from 155 to 211 bp have revealed densely compacted fibers with possible one-, two-, and three-start structures.<sup>40</sup>

Over the past few years, we have developed a mesoscale model for studying chromatin structure<sup>41–45</sup> (see Fig. 1). Our mesoscale model essentially captures the basic physics of chromatin such as its electrostatics, DNA and nucleosome mechanics, structural irregularity, and histone tail flexibility and averages out other effects: protein/DNA sequence effects, hydrogen bonding, atomistic fluctuations, and solvation effects.<sup>45</sup> The model details, including simulation methods, validation studies, and prior applications, were recently presented in the work of Arya and Schlick,<sup>45</sup> where the role of histone tails in compacting fiber structure was analyzed. In our recent study in collaboration with experimentalists,<sup>46</sup> we examined the effect of LHs and divalent ions (the latter by a first-order approximation) on chromatin structure. The cross-linking experimental procedure and modeling both provided evidence for an organized, compact zigzag model at monovalent salt with LH and an ordered zigzag accented with some bent linker DNA at divalent salt conditions. The heterogeneous nature of chromatin emerged as an important feature that helps condense chromatin as well as possibly transition the 30-nm fiber into higher-order condensed forms.<sup>46</sup> Many other modeling studies of nucleosomes and oligonucleosomes have been reported, for example, Refs. 25,26, and 47–54. Each model is suitable for a different level of questions and resolution, and all have advanced our understanding of chromatin organization and experimental structures.

Here, we present results of our mesoscale chromatin model for chromatin structure as a function of

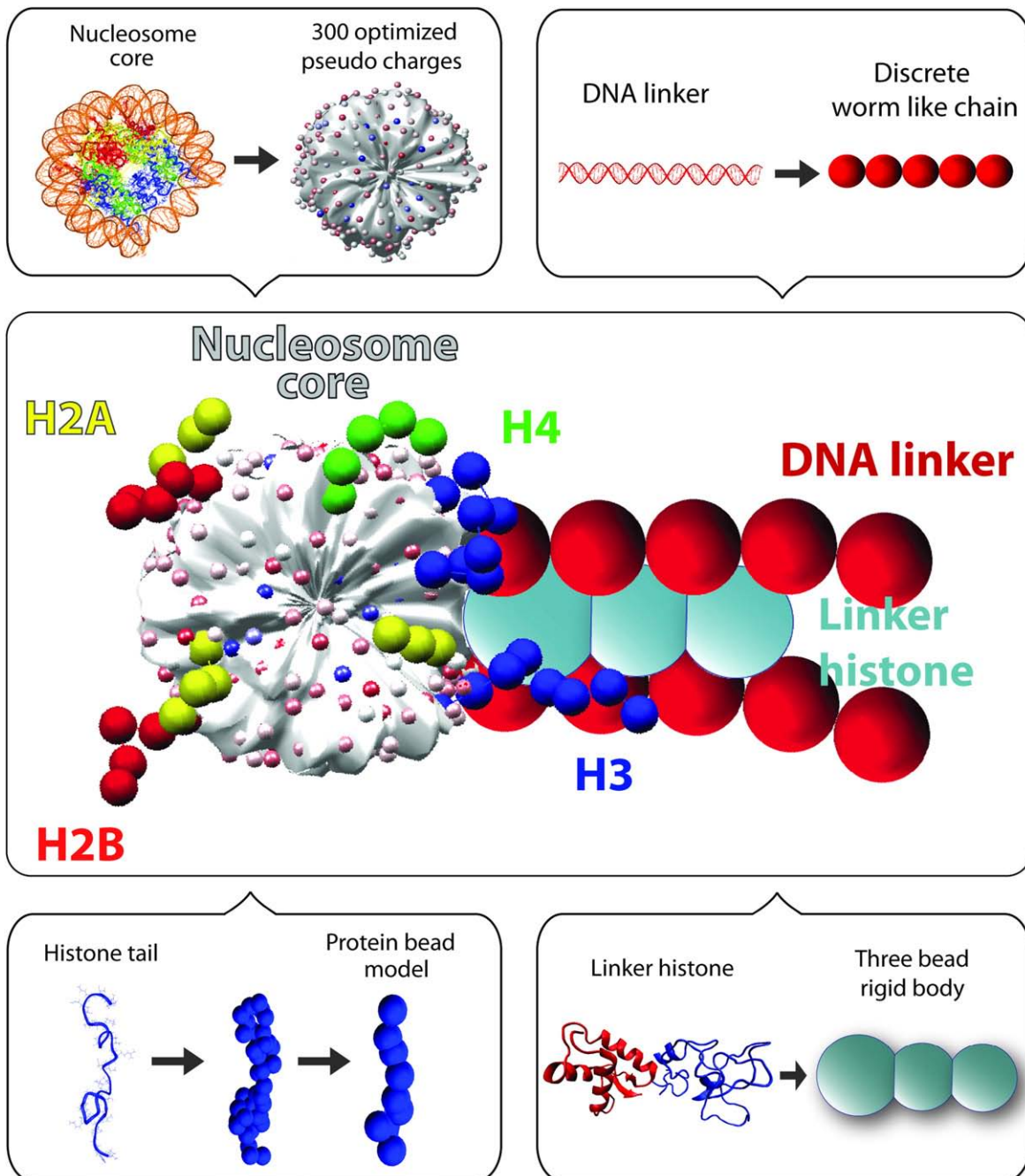


**Fig. 1.** Mesoscale model of the basic chromatin building block. The nucleosome core surface with wrapped DNA without histone tails is modeled as an irregularly shaped rigid body with 300 optimized pseudo-surface charges (smallest white, pink, magenta, and blue spheres). The linker DNA (large red spheres) is treated using the discrete worm-like chain model. The histone tails are coarse grained as bead models (medium red, yellow, green, and blue spheres). The LH is modeled as three charged beads rigidly connected to the nucleosome (turquoise spheres).

269 linker DNA length (NRL=173, 182, 191, 200, 209,  
 270 218, or 226 bp) and LH. For each condition, we start  
 271 simulations from solenoid and zigzag structures and  
 272 compare structural features of the converged fibers.  
 273 We use mainly 24-core arrays as typically studied in  
 274 a laboratory,<sup>55</sup> at monovalent ion concentrations of

0.15 M. Additionally, we show representative  
 275 results for different monovalent ion concentrations,  
 276 with/without  $Mg^{2+}$ , for three NRLs, as well as  
 277 representative snapshots of 48-core arrays. The  
 278 effect of magnesium ions on a fixed linker DNA  
 279 length was presented separately,<sup>46</sup> and an initial  
 280

t2.2 **Table 2.** DNA twisting angles as a function of NRL

t2.3	Number of segments, $n_s$							
	3	4	5	6	7	8	9	
t2.4								
t2.5	Linker length, $l_{R}^{\text{DNA}}$ (bp)	26.47	35.29	44.12	52.94	61.76	70.59	79.41
t2.6	Closest NRL (bp)	173	182	191	200	209	218	226
t2.7	Number of turns, $\tau_{n_s}$	2.57	3.43	4.28	5.14	6	6.85	7.71
t2.8	Deviation from integral turns, $\text{int}(\tau_{n_s}) - \tau_{n_s}$	-0.57	-0.43	-0.28	-0.14	0	-0.85	-0.71
t2.9	Whole linker twist, $n_s \varphi_{n_s}$ ( $=\text{int}(\tau_{n_s}) - \tau_{n_s}$ ) ( $^\circ$ )	154.82	205.20	259.20	309.60	0	54.00	104.40
t2.10	Whole linker twist, $n_s \varphi_{n_s}$ (radian $\text{radian} \in [-\pi, \pi]$ )	2.7021	-2.7018	-1.7593	0.8778	0	0.9425	1.8221
t2.11	Twist per segment, $\varphi_{n_s}$ (rad)	0.9007	-0.6754	-0.3519	-0.1463	0	0.1178	0.2025

281 study for two NRL values with divalent ions was  
282 presented elsewhere.<sup>56</sup>

283 Our present results show that nucleosome arrays  
284 with short NRL tend to fold into conformations with  
285 intense two-start interactions regardless of LH  
286 presence. Specifically, arrays with very short DNA  
287 linkers (173 bp), with and without LH, and arrays  
288 with short DNA linkers (182 bp) without LH, form  
289 narrow ladder-like structures in which cores  $i$   
290 interact mainly with their  $i\pm 1$  and  $i\pm 2$  neighbors.  
291 Arrays with short DNA linkers (182 bp) and LH  
292 form slightly thicker fibers with intense  $i\pm 2$  and  $i\pm 3$   
293 contacts.

294 The presence of LH (roughly the length of 30 bp<sup>49</sup>)  
295 has the strongest structural effect on arrays with  
296 medium NRL (i.e., for NRL 191–209 bp). In these  
297 arrays, the linker DNA length is not much greater  
298 than twice the LH length, and this promotes  
299 formation of the rigid stem. Independent of the  
300 starting (solenoid or zigzag) conformation, arrays  
301 with medium NRL and LH fold into compact two-  
302 start configurations characterized by strong  $i\pm 2$  and  
303 moderate  $i\pm 5$  interactions, which reflect their tightly  
304 packed two-start structure. This result suggests that  
305 by promoting the formation of the DNA stem for  
306 medium-sized DNA linkers, LH straightens and  
307 stiffens the DNA linkers and in turn destabilizes  
308 solenoid-like features.

309 Our investigations also indicate that, in the  
310 absence of LH, medium (191 to 209 bp) to long  
311 (218 to 226 bp) NRLs encourage chromatin struc-  
312 tural heterogeneity. Chromatin fibers with these  
313 DNA linkers without LH fold into loose structures  
314 with either solenoid-like or zigzag-like features. LH  
315 cannot prevent long DNA linkers from bending  
316 in their middle section and, thereby, promotes a  
317 wide variety of nucleosome neighbors to come  
318 into close contact. Arrays with very long linkers  
319 (NRL=226 bp) and LH can adopt either a topology  
320 with dominant zigzag features characterized by  
321 strong  $i\pm 2$  and  $i\pm 5$  contacts or a heteromorphic  
322 topology in which  $i\pm 3$  and  $i\pm 5$  neighbors interact  
323 intensely followed by  $i\pm 2$  and higher-order pairs.  
324 The heterogeneous structure of longer NRL arrays  
325 makes packing into a tight fiber architecture more  
326 difficult due to their much larger accessible config-  
327 urational space.

We also address the role of histone tails for 328  
various NRLs. We show that the tails may be 329  
evolutionary optimized for NRL between 191 and 330  
209 bp, which are the lengths usually encountered in 331  
nature. 332

333 Finally, we also show that fiber compaction 334  
increases with increasing monovalent ion concen- 335  
tration and inclusions of divalent ions for medium to 336  
long NRL, where the linker length is long enough to 337  
reorganize the nucleosomes to allow close spatial 338  
proximity while also avoiding steric clashes. 339

## Results 339

### Overall analyses 340

341 For each NRL we examine (Table 2), we perform a 342  
thorough analysis for 24-core oligonucleosomes at 343  
monovalent salt concentration ( $C_S$ ) of 0.15 M. For 344  
each NRL, we use four conditions (combinations of 345  
interdigitated solenoid or zigzag starting forms 346  
with/without LH; see Supplemental Fig. S1 for 347  
starting forms). For each of these four conditions, 12  
348 trajectories of length 35 to 50 million steps are  
349 performed with combinations of 4 random initial  
350 seeds and 3 twist deviations ( $0, \pm 12^\circ$ ) about the  
351 mean DNA twist (see Table 2). Our MC simulations  
352 converge rapidly as indicated by convergence of  
353 global and local quantities (see Fig. S2) as also  
354 analyzed previously.<sup>56</sup> We use the last 5 million  
355 steps for ensemble averages and statistical analyses  
356 (Data collection). For visualization purposes, we  
357 additionally conduct a limited number of simula-  
358 tions for 48-core oligonucleosomes, as shown in  
359 Figs. 2 and 3, as a function of NRL. We also conduct  
360 simulations in three other conditions for selected  
361 NRLs: low monovalent salt:  $C_S=0.01$  M; high  
362 monovalent salt:  $C_S=0.2$  M; and both monovalent  
363 and divalent ions:  $C_S=0.15$  M monovalent salt with  
364 moderate divalent ions, to obtain general trends of  
365 altered ionic environment.

366 Important to our overall analysis is a description  
367 of the internal organization of nucleosomes (see Fig.  
368 3 for illustration of contacts) in a chromatin fiber by  
369 a two-dimensional interaction-intensity matrix,  $I'(i,j)$

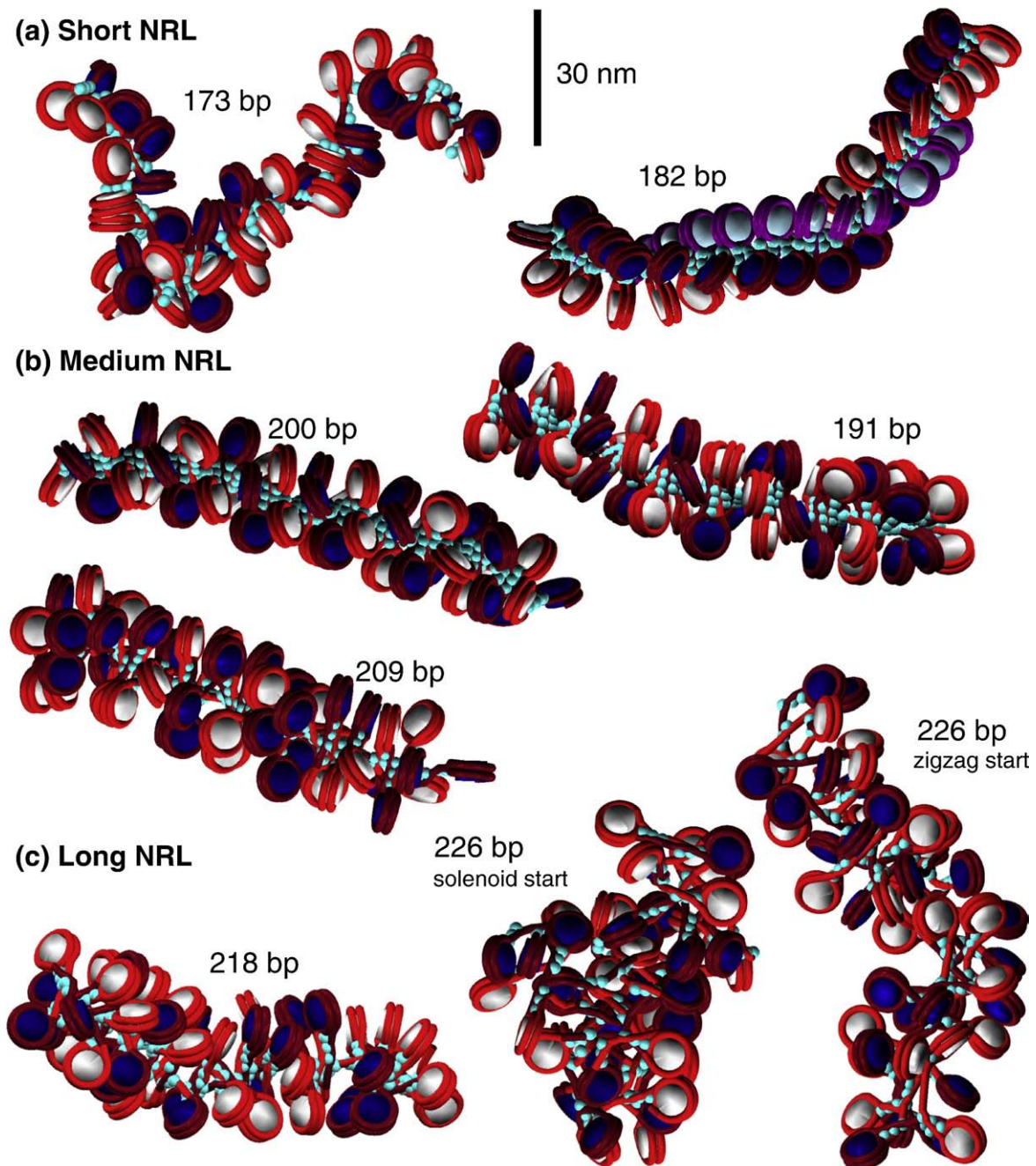


**Fig. 2.** Space-filling models based on MC simulations of 48-unit oligonucleosome chains of all NRL compacted at 0.15 M monovalent salt with LH (turquoise beads). Alternating nucleosomes are colored white and navy, with corresponding wrapped DNA as red and burgundy. In the 182-bp array, nucleosomes  $i$ ,  $i+1$ , and  $i+2$  are colored white, navy, and light blue, with corresponding DNA as red, burgundy, and purple, to highlight the three-start structure. LH is turquoise.

370 (Supplemental Fig. S3). This matrix measures the  
 371 intensity of histone-tail-mediated interactions  
 372 between nucleosomes  $i$  and  $j$ , as described in detail  
 373 in Internucleosome interactions. For an  $N_C$ -core array,  
 374 the accompanying normalized one-dimensional projection  
 375  $I(k) = \sum_{i=1}^{N_C} I(i, i \pm k) / \sum_{j=1}^{N_C} I(j)$  depicts

the relative intensity of interactions between nucleo- 376  
 somes separated by  $k$  neighbors (Fig. 4).<sup>43</sup> Thus, the 377  
 ideal two-start zigzag configuration has dominant 378  
 $i \pm 2$  and moderate  $i \pm 5$  interactions (Fig. S1),<sup>22</sup> while 379  
 the ideal 6-nucleosomes-per-turn solenoid model 380  
 has dominant  $i \pm 1$  and  $i \pm 6$  interactions (see Fig. 3 381

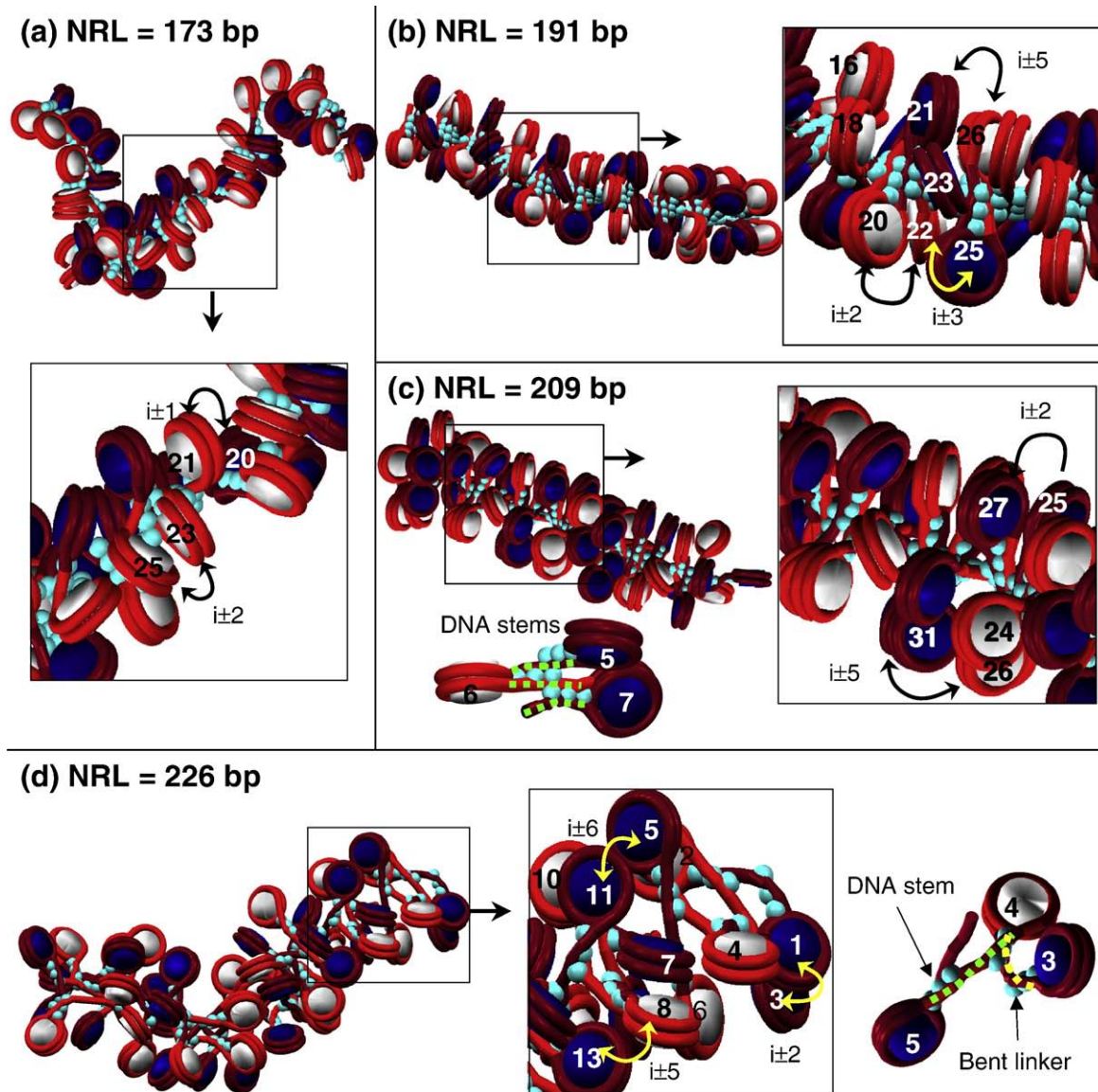


**Fig. 3.** Selected models from Fig. 2 analyzed for internucleosome contacts and linker DNA bending. (a) Arrays with very short NRL (173 bp) and LH fold into a narrow structure with low linear packing ratio regardless of LH presence. (b and c) Arrays with medium-length NRL (191 and 209 bp) and LH fold into zigzag structures with straight linkers and DNA linker stems. (d) Arrays with longest NRL (226 bp) fold into irregular structures with both DNA stems and bent linkers. Alternating nucleosomes are colored white and navy, with correspondingly wrapped DNA as red and burgundy. LH is turquoise.

382 in Ref. 46). The interdigitated solenoid model, 383 which we use here, is characterized by  $i \pm 5$  and  $i \pm 6$  384 interactions<sup>37,57</sup> (Fig. S1).

385 Other quantities that characterize fiber structure 386 are the ensemble averages of the following: dimer 387 distance between consecutive nucleosomes, triplet 388 distance between  $i \pm 2$  nucleosome neighbors, DNA 389 bending angle between the vector 'leaving' one 390 nucleosome and the vector 'entering' its consecutive 391 neighbor (as introduced in Ref. 45), triplet angle 392 between the geometric centers of three consecutive

nucleosomes, and dihedral angle between the 393 geometric centers of four consecutive nucleosomes. 394 All these quantities are detailed in [Bending, triplet, 395 and dihedral angles](#) and [Supplemental Fig. S4](#). The 396 dimer and triplet distances reflect the proximity of 397  $i \pm 1$  and  $i \pm 2$  neighbors, respectively; zigzag struc- 398 tures are characterized by smaller triplet than dimer 399 distances, and for solenoid forms, it is the reverse. 400 The bending angle helps describe linker DNA 401 bending: the angle is larger for solenoid fibers 402 with bent linkers than for zigzag arrays. Classic 403

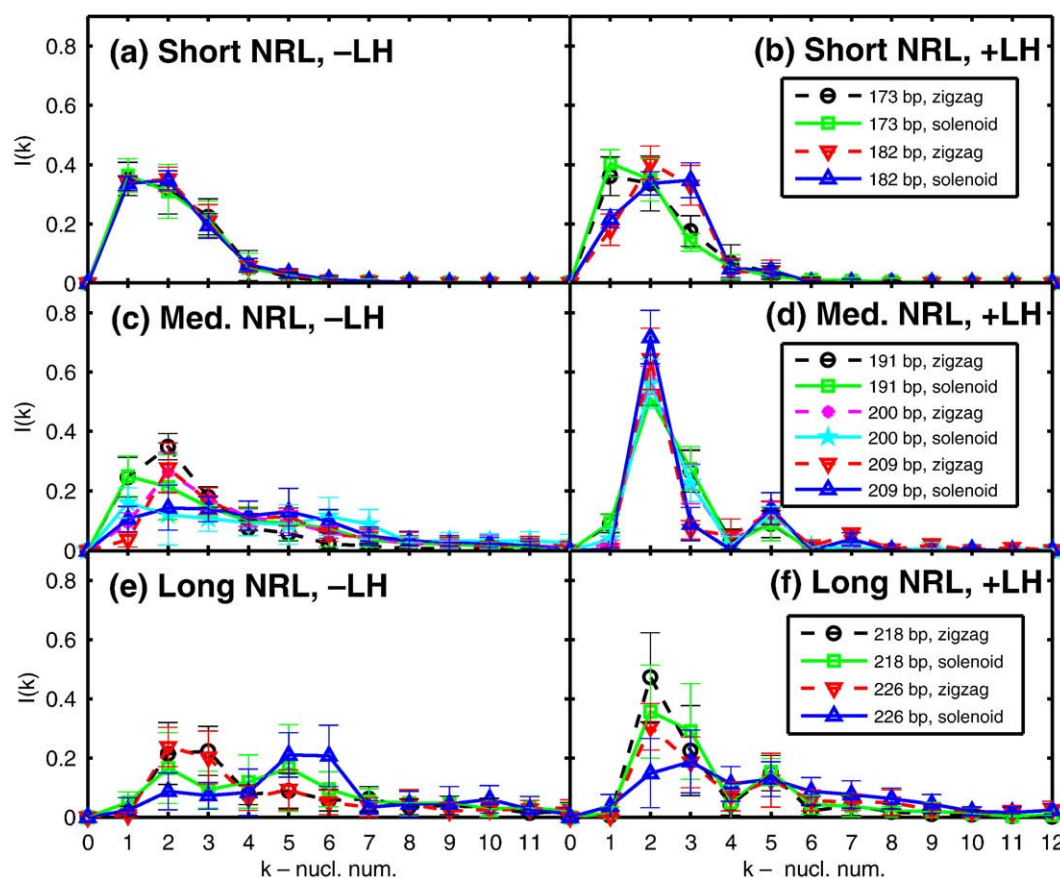


**Fig. 4.** Internucleosomal interaction patterns at 0.15 M monovalent salt. Interaction intensities *versus* nucleosome position separation  $k$  for 24-core arrays: (a) short NRL (173 and 182 bp) without LH, (b) short NRL (173 and 182 bp) with LH, (c) medium NRL (191, 200, and 209 bp) without LH, (d) medium NRL (191, 200, and 209 bp) with LH, (e) long NRL (218 and 226 bp) without LH, and (f) long NRL (218 and 226 bp) with LH. Results for trajectories started from idealized zigzag and interdigitated solenoid conformations are shown separately.

404 zigzag fibers also have small average triplet angles  
 405 that allow strong  $i \pm 2$  interactions, while solenoid  
 406 fibers have very wide triplet angles by construction.  
 407 The average dihedral angle is  $180^\circ$  when the  
 408 distance between nucleosomes  $i$  and  $i \pm 3$  is maximal.  
 409 As the fiber components reorient bringing nucleo-  
 410 somes  $i$  and  $i \pm 3$  closer, this dihedral angle decreases.  
 411 Thus, while small dihedral angles indicate close  
 412 proximity of four consecutive nucleosomes, large  
 413 dihedral angles signal weak interactions between  
 414 nucleosomes separated by two or more neighbors.

415 Additionally, we describe the degree of compac-  
 416 tion of the oligonucleosomes by the sedimentation  
 417 coefficient ( $S_{20,w}$ ), overall nucleosomal packing  
 418 ratios (number of nucleosomes per 11 nm of fiber  
 419 length), fiber width, fiber volume, percentage of  
 420 ‘filled’ fiber volume, and curvature of the fiber axis  
 421 (see Calculation of sedimentation coefficients and  
 422 Calculation of fiber packing ratio, curvature, and  
 423 volume for details).

424 Figures 4, 5, and 6 show the main results for  
 425 24-core arrays: internucleosome interaction patterns

and geometrical features. Figure 7 assesses chromatin 426  
 compactness as a function of the salt concentra- 427  
 tion, and Fig. 8 describes tail-mediated interactions. 428  
 All these features will be detailed in the subsections 429  
 below. 430

### Overall fiber structure as a function of a DNA 431 linker length 432

Overall, we recognize three separate NRL ranges: 433  
 (a) short NRL: 173 bp to 182 bp, (b) medium NRL: 434  
 191 bp to 209 bp, and (c) long NRL: 218 to 226 bp. 435  
 The fibers with shortest NRL fold into narrow 436  
 ladder-like structures regardless of the presence of 437  
 LH and show no increase in packing ratio upon the 438  
 addition of LH. Arrays with medium NRL with LH 439  
 strongly resemble shapes of highly compacted 440  
 arrays visualized by the EM-assisted nucleosome 441  
 interaction capture technique.<sup>46</sup> These are regu- 442  
 larly shaped with dominant two-start zigzag 443  
 configurations. Arrays with medium NRL also 444  
 show the highest linear packing density increase 445



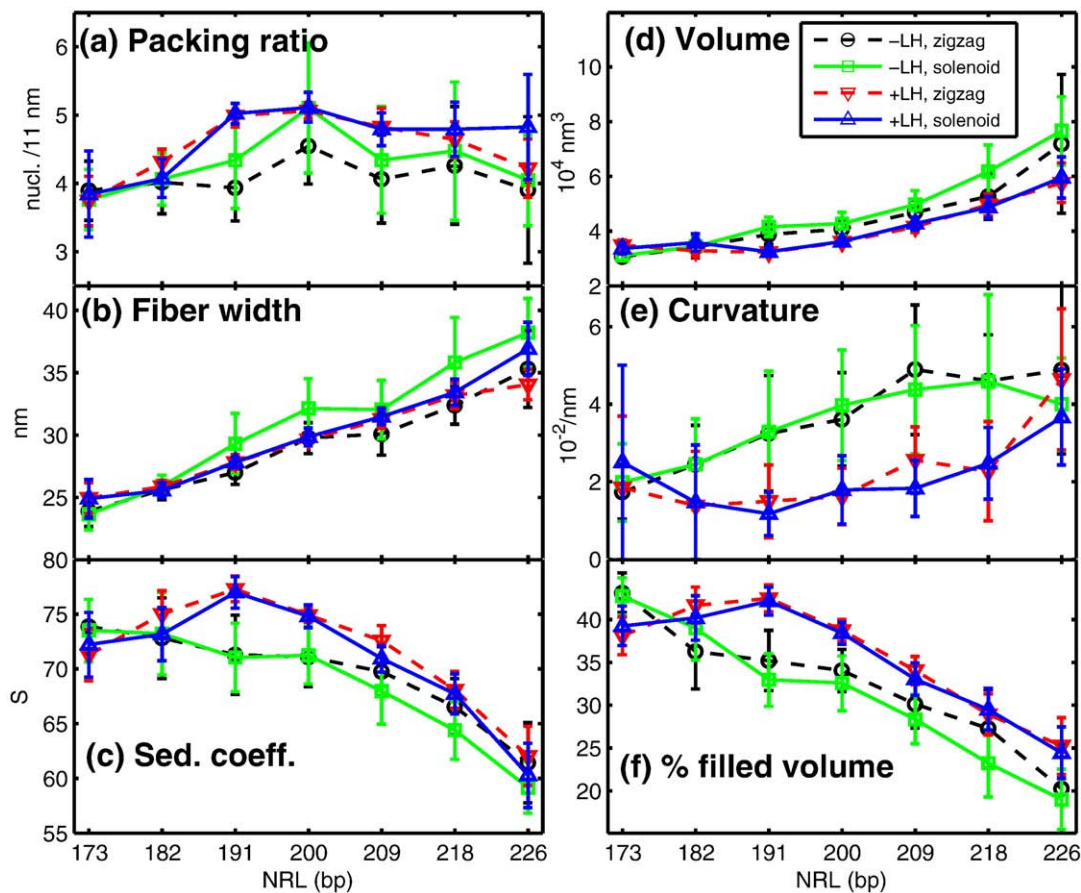


**Fig. 5.** Chromatin fiber dimensions as a function of NRL. (a) Nucleosome linear packing ratio, (b) fiber width, and (c) sedimentation coefficients, (d) fiber volume, (e) fiber curvature, and (f) percentage of filled volume, all as functions of NRL for 24-core oligonucleosomes. Results shown for simulations started from zigzag configuration and modeled without LH, started from solenoid without LH, started from zigzag with LH, and started from solenoid with LH at 0.15 M monovalent salt. Nucleosome packing ratios are measured as the number of nucleosomes per 11 nm of fiber axis length. The fiber width is calculated as an average distance of nucleosomes (+nucleosome half radius) from the fiber axis (Supplemental Fig. S6).

446 and sedimentation coefficients upon addition of  
 447 LH. For arrays with medium NRL, LH leads to a  
 448 moderate increase in the fiber diameter. In contrast,  
 449 fibers with long NRL with LH have a more  
 450 heterogeneous structure, with both bent DNA  
 451 linkers and straight DNA linkers due to stems  
 452 formed by the interaction of the exiting/entering  
 453 DNA with LH. The DNA linkers tend to bend  
 454 because the total length of two LHs ( $\sim 60$  bp)  
 455 is shorter than the length of a single DNA linker (see  
 456 Fig. 3 for an illustration of a 226-bp array, where  
 457 linker DNA length is 79 bp).

#### 458 Short NRL: 173 and 182 bp

459 Our simulations suggest that chromatin fibers  
 460 with the shortest (NRL=173 bp) DNA linkers, both  
 461 with and without LH, fold into a two-start ladder-  
 462 like structure characterized by strong  $i \pm 1$  and  $i \pm 2$

interactions (Figs. 3a and 4a and b), a low linear  
 463 packing density ( $\sim 3.8$  nucleosomes/11 nm; Fig. 5a),  
 464 and a narrow width ( $\sim 24$ – $25$  nm; Fig. 5b), regard-  
 465 less of the starting conformation. Further support for  
 466 a ladder-like structure for these arrays comes from  
 467 the large dihedral angle observed regardless of LH  
 468 presence (Fig. 6d).  
 469

The interaction patterns for arrays with 182-bp  
 470 NRL without LH also show strong  $i \pm 1$  and  $i \pm 2$   
 471 contacts and large dihedral angles ( $\sim 80^\circ$ ), resem-  
 472 bling the arrays with the shortest linker DNA  
 473 described above (Figs. 4a and 6d).  
 474

The addition of LH to the 182-bp arrays slightly  
 475 straightens the linker DNAs (as indicated by a small  
 476 decrease in the bending angles; Fig. 6c) and  
 477 reorganizes the nucleosome contacts, increasing  
 478 the relative intensity of  $i \pm 2$  and  $i \pm 3$  interactions at  
 479 the expense of that of  $i \pm 1$  (Fig. 4b). This indicates  
 480 that 182-bp arrays with LH fold into a fiber that  
 481

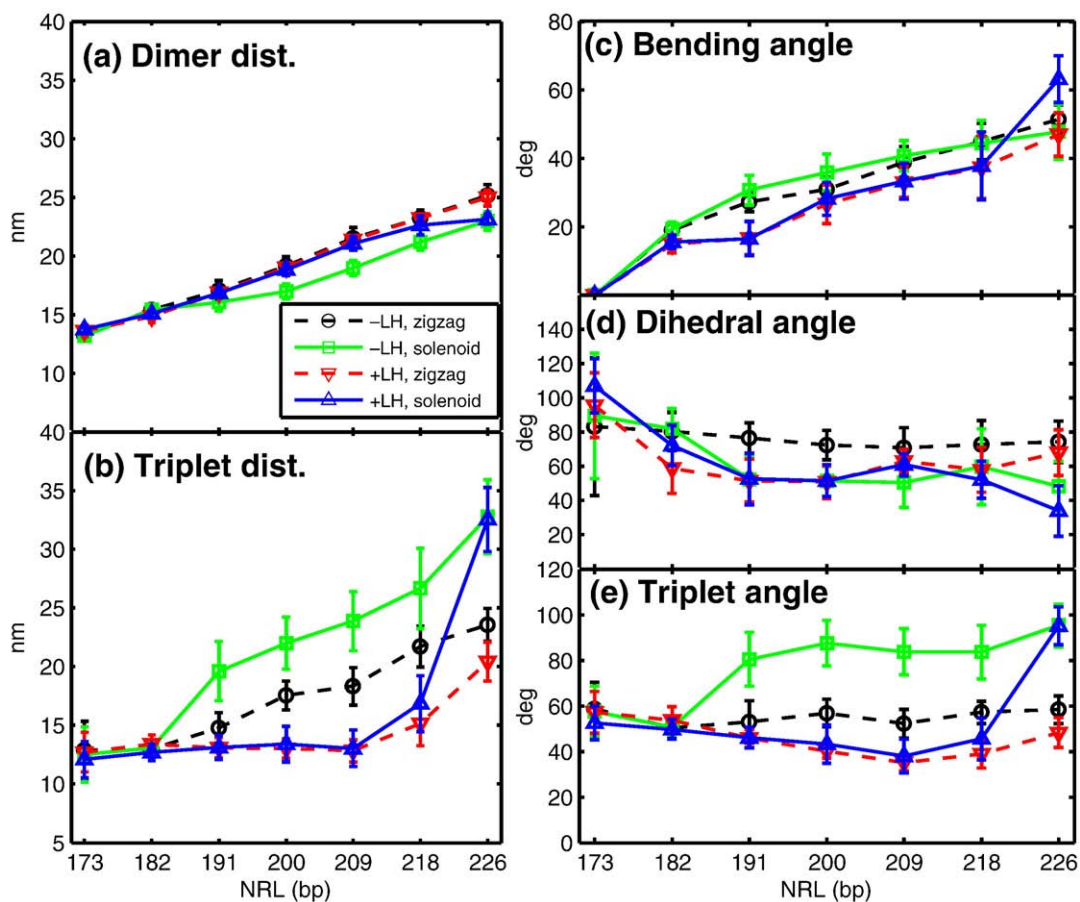


**Fig. 6.** Geometric parameters for different NRL systems 24-core arrays: (a) dimer distances (between  $i+1$  nucleosome neighbors), (b) triplet distances (between  $i+2$  neighbors), (c) bending angles, (d) dihedral angles, and (e) triplet angles for 24-core arrays at 0.15 M monovalent salt. The bending angle is defined as the angle between vectors passing through the first two and last two DNA linker beads. The triplet angle is an angle between the geometric centers of three consecutive nucleosomes. The dihedral angle is the angle between two planes defined by four consecutive nucleosomes (see Supplemental Fig. S4).

interconverts between a two-start and a three-start structure. LH also reduces the dihedral angles to  $\sim 65^\circ$  consistent with the increase of  $i\pm 3$  contacts (Fig. 6d). The addition of LH, however, does not increase fiber compaction significantly; the packing ratios, sedimentation coefficients, fiber width, fiber volume, and percentage of filled volume remain almost constant (Fig. 5). The triplet angles also remain constant ( $50\text{--}60^\circ$ ; Fig. 6e) regardless of the starting conformation.

#### 492 Medium NRL: 191, 200, and 209 bp

493 The structure of medium-NRL arrays depends on  
494 the presence of LH. Without LH, these arrays exhibit  
495 structural heterogeneity. When started from zigzag  
496 configurations, they converge to arrays with irreg-  
497 ular zigzag-like features: intense  $i\pm 2$ , notable  $i\pm 1$ ,  
498 and higher contacts (Fig. 4c); medium dihedral

angles ( $\sim 70^\circ$ ; Fig. 6d); and medium triplet angles  
( $< 65^\circ$ ; Fig. 6e). When started from solenoid config-  
urations, they converge to structures with irregular  
solenoid-like characteristics: intense  $i\pm 1$  and  $i\pm 2$   
contacts combined with multiple other prominent  
higher-order interactions (Fig. 4c), large triplet  
angles ( $> 80^\circ$ ; Fig. 6e), and smaller dihedral angles  
( $\sim 50^\circ$ ; Fig. 6d).

When LH is added to medium-NRL arrays, solenoid interactions are destabilized in favor of zigzag-like forms. Simulations started from both zigzags, and solenoids form a compact zigzag fiber with uniform features that include straight DNA linkers (reduced bending angles) that stabilize a DNA stem (see Fig. 3c for stem illustration). Independent of NRL, this zigzag fiber has dominant  $i\pm 2$  interactions and moderate  $i\pm 5$  contacts (Figs. 3b and c and 4d), consistent with smaller triplet than dimer distances (Fig. 6a and b). These fibers exhibit

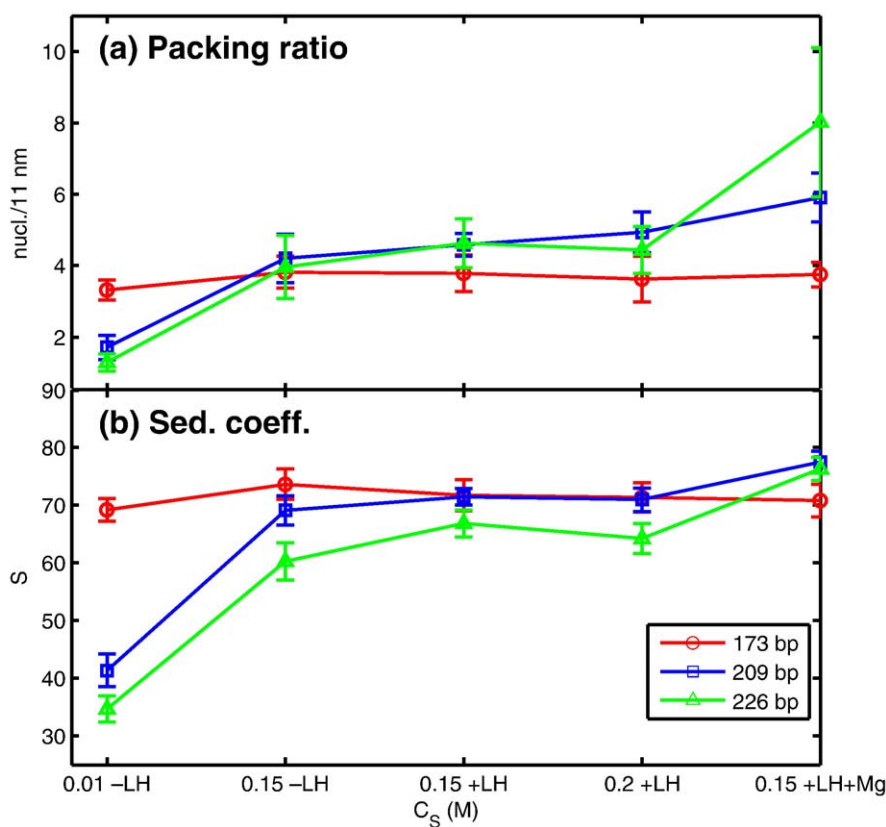


**Fig. 7.** Chromatin fiber measurements as a function of the salt environment for 24 oligonucleosomes: (a) nucleosome linear packing ratio and (b) sedimentation coefficients. Ensemble averages over trajectories started from zigzag and interdigitated solenoid configurations. The three new salt environment corresponds to monovalent  $C_S=0.01$  M without LH (-LH), monovalent  $C_S=0.2$  M with LH (+LH), and moderate monovalent salt at  $C_S=0.15$  M with LH and divalent ions (+LH+Mg).

518 the smallest dihedral ( $\sim 50^\circ$ ; Fig. 6d) and triplet  
 519 ( $< 50^\circ$ ; Fig. 6e) angles. The tightness of these medium  
 520 NRLs with LH fibers is also supported by the  
 521 relatively high packing ratios ( $\sim 5.0$  nucleosomes/  
 522 11 nm), sedimentation coefficients, and the percent-  
 523 age of filled volumes, as well as small curvature  
 524 (straighter fibers) observed in Fig. 5.

#### 525 Long NRL: 218 and 226 bp

526 Long DNA linker arrays exhibit structural diver-  
 527 sity. Without LH, both zigzag and solenoid-like  
 528 features are viable. Namely, arrays started from  
 529 zigzag conformations converge to an irregular two-  
 530 start structure with dominant  $i\pm 2$  and  $i\pm 3$  inter-  
 531 actions and intense  $i\pm 5$  contacts (Fig. 4e), as well as  
 532 medium dihedral and triplet angles (Fig. 6); arrays  
 533 started from solenoid converge to structures with  
 534 zigzag and solenoid characteristics. Specifically, the  
 535 218-bp arrays started from solenoid possess equally  
 536 intense  $i\pm 2$  and  $i\pm 5$  interactions, while the 226-bp  
 537 arrays have stronger  $i\pm 5$  and  $i\pm 6$  interactions  
 538 followed by  $i\pm 2$  contacts (Fig. 4e). Both have small

dihedral angles and large triplet angles (Fig. 6),  
 characteristic of solenoid conformations.

540  
 541 The effect of LH in favoring a zigzag structure  
 542 weakens for long NRL. This is because the DNA  
 543 linker is much longer than twice the size of the LH.  
 544 While LH still triggers the formation of a DNA stem,  
 545 increasing the intensity of  $i\pm 2$  interactions (Fig. 4f),  
 546 it cannot prevent the long DNA linkers from bending  
 547 in their middle section (see Fig. 3d for illustration),  
 548 and this promotes a wider range of nucleosome  
 549 interactions. The 218-bp arrays with LH started from  
 550 zigzag and solenoid conformations converge to  
 551 different structures with dominant  $i\pm 2$  and intense  
 552  $i\pm 3$  and  $i\pm 5$  interactions. The different relative  
 553 intensities of these interactions between the struc-  
 554 tures started from solenoid and zigzag reflect the  
 555 structural diversity favored by long DNA linkers.

556 Thus, we observe that, as the NRL increases, the  
 557 effectiveness of LH in forming a DNA stem and  
 558 promoting two-start contacts decreases. In our  
 559 longest NRL systems (226 bp) with LH, both  
 560 solenoid-like and zigzag-like characteristics are  
 561 viable (Fig. 4f). When started from zigzag, the 226-

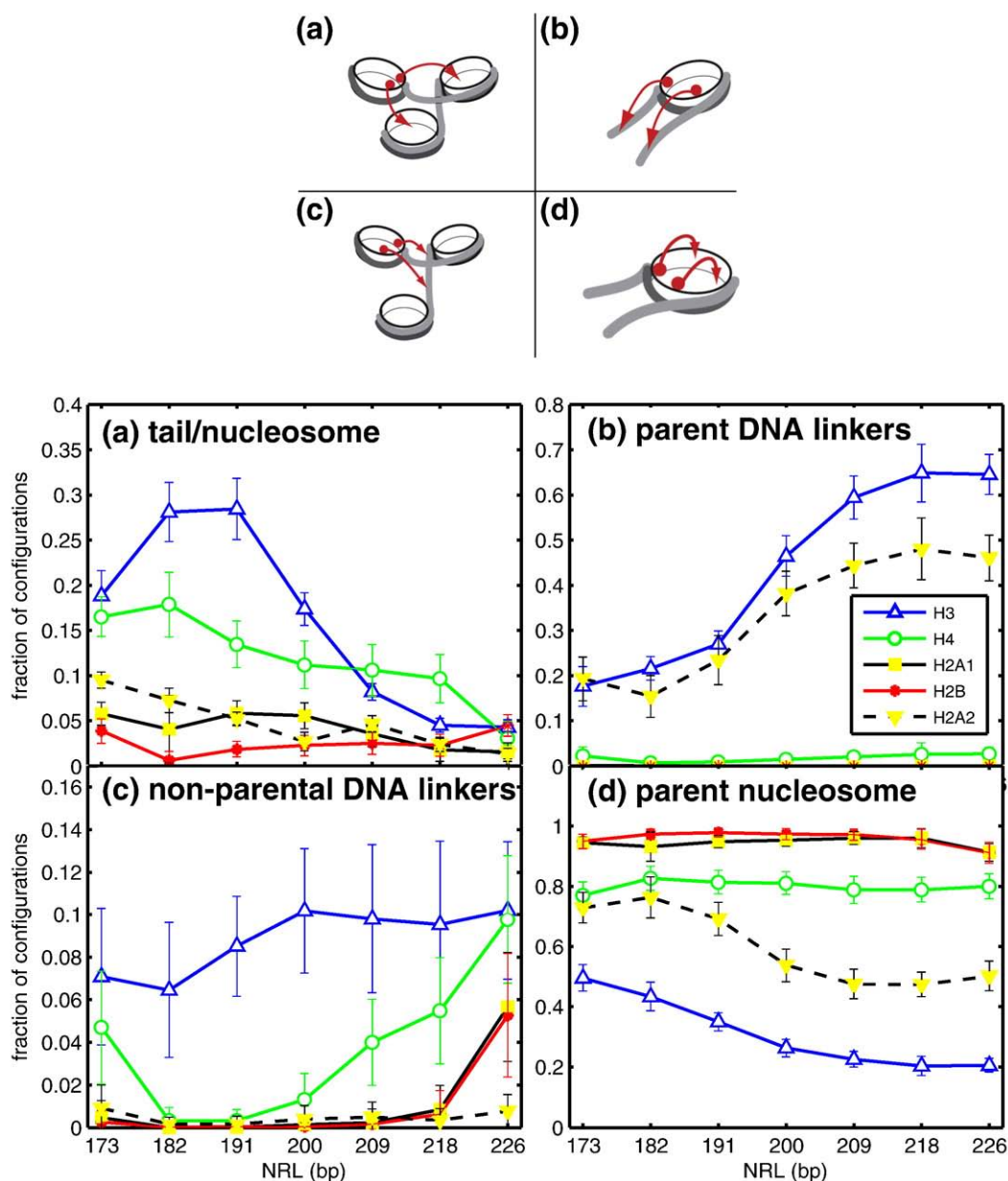


**Fig. 8.** Frequency analyses and cartoon images of different tail interactions in 24-core oligonucleosomes with LH at 0.15 M monovalent salt: (a) nucleosome/nucleosome interactions, (b) interactions with parent linker DNA, (c) interactions with non-parent DNA linkers, and (d) interactions with parent nucleosome. H2A<sub>1</sub> and H2A<sub>2</sub> denote N-termini and C-termini, respectively, of the H2A tails.

562 bp arrays with LH converge to a structure with  
 563 dominant  $i\pm 2$  interactions, intense  $i\pm 5$  contacts, and  
 564 small dihedral and triplet angles, all of which are  
 565 consistent with a compact zigzag structure. How-  
 566 ever, when started from solenoid, the 226-bp arrays  
 567 with LH lead to heteromorphic structures with  
 568 zigzag interaction patterns (intense  $i\pm 3$  and  $i\pm 5$  and  
 569 strong  $i\pm 2$  contacts) but small dihedral angles ( $>40^\circ$ ;  
 570 Fig. 6d) and large triplet angles ( $>90^\circ$ ; Fig. 6e),  
 571 consistent with the solenoid form.

The long linker lengths of these fibers, however, 572  
 restrict their compaction relative to medium-NRL 573  
 fibers. This is reflected by their smaller packing 574  
 ratios, sedimentation coefficients, and percentage of 575  
 filled volume in Fig. 5. 576

#### LH role 577

As discussed above, the interaction patterns and 578  
 linear packing density (Figs. 4a and b and 5) of the 579

shortest linker arrays (NRL = 173 bp) weakly depend on the presence of the LH because the LH's length is longer than the DNA linker and the DNA stem cannot form. As the NRL increases to 182 bp, the LH induces DNA stem formation<sup>7</sup> (Fig. 2) because the DNA linker and LH become comparable in size. However, as for the 173-bp arrays, LH cannot increase fiber compaction; the DNA linkers in arrays with these low NRL values reorient themselves to avoid collision with neighboring cores as well as linker DNAs when LH is present. The nucleosome reorientation also prohibits the formation of one-start solenoid structures.

LH has the strongest influence on arrays with medium NRL (NRL between 191 and 209 bp). Addition of LH to arrays with this NRL range encourages a zigzag organization and increases compaction. These linker lengths are sufficiently long to form a DNA stem and consequently reorganize in a compact zigzag structure avoiding steric clashes (Fig. 3b and c).

The effect of LH is smaller for arrays with longer NRL values (218 and 226 bp) because the LH's length is less than half the DNA linker's length. This allows the base pairs in the center of the linker DNA to bend in the folded fibers (Figs. 3d and 6c). This bending, in turn, increases the  $i\pm 3$  and  $i\pm 5$  interactions at the cost of the  $i\pm 2$  interactions.

### 608 Role of ionic concentration

The results reported above are for 0.15-M monovalent salt concentration ( $C_S$ ). The compaction of chromatin depends on the ionic environment. To show that fiber compaction increases in high monovalent ionic concentrations and upon addition of divalent ions, we present representative data for 24-core arrays in three additional conditions: (i) low monovalent salt ( $C_S=0.01$  M) without LH, (ii)  $C_S=0.2$  M with LH, and (iii)  $C_S=0.15$  M with  $Mg^{2+}$  and LH. The divalent ion treatment is a simple first-order approximation as introduced in Ref. <sup>45</sup>, implemented by reducing the DNA persistence length to 30 nm and allowing the DNA linker beads to touch one another (see details in [Computational Methods](#)). Figure 7 shows the increase in packing ratio and sedimentation coefficients as a function of the salt environment for NRL=173, 209, and 226 bp. Representative snapshots for 48-core arrays are presented in [Supplemental Fig. S5](#) to illustrate the change in compaction at different salt environments. The compaction of the 173-bp arrays does not increase because the linkers are too short. The compaction in the 182-bp and 226-bp arrays increases at higher monovalent salt and most significantly upon addition of magnesium ions. Thus, we expect the values shown in [Figs. 4–6](#) to change accordingly in these altered salt environments.

### Role of histone tails

Three types of tail interactions are responsible for bridging contacts: (i) nucleosome/nucleosome interactions, (ii) tail interactions with parental DNA, and (iii) tail interactions with non-parental DNA. The H3/H4 tails are known to have a key role in chromatin compaction<sup>43,58–66</sup> while H2A<sub>1</sub>/H2A<sub>2</sub>/H2B tails are involved in histone core aggregation,<sup>67</sup> transcription control, and possible mediation of inter-fiber interactions due to their position on the periphery of the nucleosome<sup>43</sup> (H2A<sub>1</sub> and H2A<sub>2</sub> are, respectively, the N-termini and C-termini of the H2A tails).

In our simulations, we dissect the role of the different tails in fiber-bridging contacts as a function of the NRL by measuring the fraction of configurations that specific tails are attached to a chromatin component (i.e., parent core, non-parent core, parent DNA linker, or non-parent linker). A tail is considered to be attached to a component if it is closer than the excluded volume distance for tail/particle interactions (1.8 nm) (see [Tail interactions](#)).

#### Tail/nucleosome interactions (H3 and H4 dominant)

For compact chromatin with LH and linkers comparable to the LH size (173–200 bp), the H3 tails mediate the largest number of internucleosomal contacts, followed by H4 (Fig. 8a). In these arrays, the H3 and H4 tails spend 19–28% and 11–18% of their time interacting with other cores, respectively. The time spent by tails mediating internucleosome interactions can be analyzed in light of the internucleosomal contact patterns (Fig. 4). In the 173-bp arrays with LH, nucleosomes spend 39% of time in the vicinity of their immediate sequential neighbors ( $i\pm 1$ ) and thus 61% with  $i\pm 2$  and higher contacts (Fig. 4b).

As NRL increases to 200 bp, the nucleosomes spend 81–97% of the time interacting with  $i\pm 2$  and higher neighbors (Fig. 4c). Interactions with immediate neighbors are not essential for fiber bridging in moderate-NRL arrays because their DNA linkers hardly bend. Effectively, this means that the H3 tails in 173-bp arrays spend only 12% of the time in contact with  $i\pm 2$  and higher neighbors, while for the 182, 191, and 200 bp with LH fibers, they spend 14%, 26%, and 16% of their time mediating fiber-bridging interactions, respectively.

The interactions of H3 tails with non-parental cores diminish with the increase of the DNA linker length (Fig. 8a). The H4 tails, on the other hand, spend >10% of their time mediating internucleosome interactions in arrays with NRL up to 218 bp and take over as the most important for internucleosome interactions at 209 and 218 bp. Such internucleosome contacts contribute to fiber bridging.

693 The H3 and H4 contact probabilities in arrays with  
694 longest NRL fall to less than 5% due to looser  
695 conformations. Interactions of other tails (H2A and  
696 H2B) are negligible.

#### 697 *Interactions with parent DNA linker (H3 and* 698 *H2A<sub>2</sub> dominant)*

699 The tail interactions with parent linker DNAs are  
700 mostly mediated by the H3 and H2A<sub>2</sub> tails (Fig. 8b).  
701 Their proximity to the linker DNA, length, and  
702 highly positive charge allow them to screen the  
703 electrostatic repulsion among the negatively  
704 charged DNA linkers. Besides the dominant H3  
705 and H2A<sub>2</sub> tails, the shorter H4 tails interact  
706 moderately with parental DNA because they are  
707 close to the entry/exit positions of the parental DNA  
708 linkers. All these three types of tails, in cooperation  
709 with LH, create a positively charged region that  
710 neutralizes the negatively charged DNA linkers. The  
711 screening of the electrostatic repulsion between  
712 linkers enables formation of a DNA stem.<sup>7</sup>

713 The efficiency of the H3 tails in screening  
714 electrostatic repulsions between parental DNA  
715 linkers strongly depends on the linker length. For  
716 short NRL (173 bp), the H3 tails have intense  
717 interactions with neighboring nucleosomes by con-  
718 struction and consequently reduced interactions  
719 with parental DNA linkers. The intensity of the H3  
720 tail interactions rises with the increase of the DNA  
721 linker length and reaches a maximum for NRL  
722 between 209 and 226 bp. The lengths (4.7 nm) and  
723 placement of the H2A<sub>2</sub> tails close to the nucleosome  
724 dyad axis allow them to interact with parental DNA  
725 strongly at a wide range of linker lengths.

#### 726 *Interactions with non-parental DNA linkers* 727 *(H3 dominant)*

728 The tail interactions with non-parental DNAs in  
729 fibers with LH are mostly mediated by the H3 tails  
730 (Fig. 8c) because they are sufficiently long (12.6 nm  
731 in our model). The interaction intensity reaches its  
732 peak at NRL=200 bp. The 200 bp with LH fibers  
733 have the highest packing ratios overall and are also  
734 among the most compact as reflected by their high  
735 sedimentation coefficient.

736 Other tails are much shorter (4.7 to 7.8 nm) and  
737 positioned at the periphery of the nucleosome, and  
738 this restricts their interaction with non-parental  
739 DNA linkers.

#### 740 *Interactions with parent nucleosome*

741 The short H2A<sub>1</sub> and H2B tails are not involved  
742 significantly in fiber bridging. They spend most of  
743 the time in the vicinity of the parent nucleosome  
744 (Fig. 8d). Other tails (H2A<sub>2</sub>/H3/H4) spend less time  
745 interacting with their parent nucleosome because

they are involved in interactions with other nucleo- 746  
somes and with DNA. 747

#### Configurational homogeneity 748

749 As discussed above, the structural organization of  
750 chromatin can be characterized through the analysis  
751 of the spatial orientation of consecutive nucleosomes  
752 (two, three, and four; see *Bending, triplet, and*  
753 *dihedral angles* and *Supplemental Fig. S4*). In a  
754 compact zigzag configuration, the *i* and *i*+2 cores  
755 are close, which implies small triplet distances and  
756 angles; the straight linkers produce small bending  
757 angles, and the dihedral angles are expected to be  
758 small if the fiber is compact enough to bring  
759 nucleosomes *i* and *i*+3 into intimate contact. In  
760 comparison, a compact solenoid fiber would have  
761 small dimer distances, larger triplet distances and  
762 angles, and, if compact enough, also small dihedral  
763 angles that allow cores separated by more than two  
764 neighbors to interact.

765 Our analysis confirms that arrays with short  
766 linkers (NRL=173 bp) are homogeneous, regardless  
767 of LH presence or starting conformation; all quan-  
768 tities computed are statistically equivalent for the  
769 four conditions. As expected, these arrays show  
770 small dimer and triplet distances and medium  
771 triplet angles. Their dihedral angles are large and  
772 have wider error bars due to narrow fiber widths  
773 and short average distances between nucleosomes.  
774 The size of all error bars decreases upon the addition  
775 of LH, confirming that LH promotes structural  
776 homogeneity.

777 Arrays with medium NRL (191 to 209 bp) and LH  
778 prefer zigzag configurations characterized by smal-  
779 ler average triplet than dimer distances; small  
780 bending, triplet, and dihedral angles; and smaller  
781 error bars (Fig. 6). These quantities show that  
782 LH strongly stabilizes zigzag fiber arrangements.  
783 Medium-NRL arrays without LH are heterogeneous  
784 and can adopt loose zigzag (with smaller triplet than  
785 dimer distances, larger bending angles, medium  
786 triplet angles, and large dihedral angles) or solenoid  
787 (smaller dimer than triplet distances, larger bending  
788 angles, large triplet angles, and small dihedral  
789 angles) conformations.

790 Arrays with long NRL (218–226 bp) and LH  
791 exhibit an increased heterogeneity when compared  
792 to their shorter brethren (Fig. 6). The 218-bp arrays  
793 with LH converge to two states characterized by  
794 dominant zigzag interactions; each state has slightly  
795 different average values of the dimer and triplet  
796 distances and triplet and dihedral angles. Moreover,  
797 the higher error bars in the bending angles reflect  
798 these differences. For 226-bp arrays with LH, the  
799 large bending angles in the trajectories started from  
800 solenoid indicate that some entering/exiting DNA  
801 linkers are widely separated, with LHs not neces-  
802 sarily interacting with both parental nucleosome

803 linkers. This can be explained by the decreased  
804 ability of LHs to produce DNA stems for long DNA  
805 linkers (Fig. 3d).

806 Note that as shown in Supplemental Fig. S2, the  
807 24-core short-NRL ensembles converge by 20  
808 million MC steps, while the 24-core long-NRL  
809 systems converge by 40 million MC steps, for both  
810 starting conformations. Thus, the different viable  
811 fibers discussed above reflect actual heterogeneity  
812 in the chromatin fiber architecture and the existence  
813 of multiple minima in certain conditions rather than  
814 the lack of convergence; such variations in chroma-  
815 tin structure are expected for a floppy polymer in  
816 solution.<sup>26,46</sup> Our simulations also suggest that  
817 there is a large energetic cost for structural  
818 interconversion between solenoid and zigzag states  
819 for long NRL.

820 In sum, our results indicate that zigzag con-  
821 formations are always viable and that solenoid-like  
822 characteristics are viable in either chromatin with-  
823 out LH or in systems with long DNA linkers. Even  
824 within one form, there are substantial fluctuations  
825 in internal geometric values. Our results also  
826 support the recent experimental findings that  
827 chromatin fibers are spontaneously dynamic even  
828 when compact.<sup>68</sup>

## 829 Discussion

830 Our modeling reveals that, in the presence of LH,  
831 fibers with a wide range of NRL have strong  $i \pm 2$   
832 interactions, consistent with the classical zigzag  
833 configuration. Very short linker arrays  
834 (NRL = 173 bp) have strong  $i \pm 1$  and  $i \pm 2$  interactions  
835 with or without LH, simply by construction. They  
836 also exhibit much wider dihedral angles than the  
837 longer NRL fibers, commensurate with their narrow  
838 widths and ladder-like structure regardless of LH  
839 presence (Figs. 3, 5, and 6). These characteristics  
840 underscore the primary role of LH as a bridge  
841 between neighboring DNA linkers. Our observation  
842 is consistent with the experimentally measured  
843 stoichiometry of H1 in wild-type ES cells.<sup>3</sup> Even  
844 smaller values are found in simple unicellular  
845 organisms such as yeast.<sup>69</sup> Further, *in vivo* experi-  
846 ments show that H1 does not have a crucial role in  
847 such organisms; that is, its substantial reduction  
848 causes minor phenotypical changes.<sup>70,71</sup>

849 We also find that LH has a notable structural effect  
850 in fibers with slightly longer NRL (182 bp). Here, LH  
851 forms the DNA stem, decreasing the exposure of the  
852 DNA and enhancing the intensity of  $i \pm 2$  and  $i \pm 3$   
853 contacts. LH, however, does not increase the  
854 packing ratio or sedimentation coefficient at the  
855 moderate monovalent ion concentration considered  
856 (0.15 M).

857 For fibers with medium NRL (191 to 209 bp), LH  
858 tends to favor zigzag structures. Higher packing

859 ratios can be achieved only with fibers of medium  
860 NRL in the presence of LH. These fibers also show  
861 the highest increase in sedimentation coefficients  
862 and linear packing ratios, and the smallest dihedral  
863 angles, suggesting that LH is evolutionary opti-  
864 mized for NRL between 191 and 209 bp, most often  
865 encountered in nature.<sup>2</sup>

866 Our packing ratios are smaller than the experi-  
867 mentally reported values for several reasons. First,  
868 our model does not account for ion correlation effects  
869 beyond simple screening as discussed previously,<sup>45</sup>  
870 and most of our results correspond to moderate  
871 monovalent salt. We have shown that for medium to  
872 long NRL, the packing ratios are very sensitive to the  
873 ionic environment: higher concentrations of mono-  
874 valent salt as well as added divalent ions increase  
875 compaction significantly (Fig. 7). Second, our LH  
876 model is a simple geometric one and does not  
877 consider explicit electrostatic interactions with non-  
878 parental DNA linkers or the nucleosome or the  
879 binding–unbinding of LH. While this description  
880 accurately reproduces the most important structural  
881 role of LH—formation of the DNA stem—further  
882 model refinements could help describe these other  
883 effects. It should also be noted that experimental  
884 measurements for packing ratios are conducted  
885 manually and differ from the procedure we use  
886 (Supplemental Fig. S6). Namely, manual procedures  
887 consider the chromatin fiber as a flat two-dimen-  
888 sional object, while our procedure considers the  
889 chromatin as a three-dimensional entity.

890 The longer linker lengths (NRL = 218 bp and  
891 higher) are less often encountered in nature. Our  
892 modeling suggests that those arrays have complex  
893 internal structure with multiple stable conforma-  
894 tions and small relative packing ratios.

895 Though short DNA linkers are not desirable as  
896 they do not offer high packing density, they have  
897 one advantage over the longer linkers. Nucleosome  
898 arrays with short linkers expose their DNA to  
899 transcription and replication machinery; their  
900 higher standard deviations of dihedral angles  
901 indicate that they are less stable and more prone to  
902 opening, as experimentally shown.<sup>68</sup> The ladder-like  
903 structures require just one or two displacements to  
904 expose DNA to the environment.

905 Facile access to the DNA may be important in  
906 simpler organisms, such as yeast, slime molds, and  
907 ciliates, which have a very short life span and very  
908 high reproduction rates.<sup>2,72,73</sup> These organisms  
909 require access to all protein sequences in one cell.  
910 Interestingly, chromatin can fold into a compact  
911 structure without LH when linkers are short.<sup>28</sup>

912 Simpler organisms also have smaller concentra-  
913 tions of LH per nucleosome than found in higher  
914 organisms.<sup>3</sup> Moreover, covalent histone tail modifi-  
915 cations that increase the attraction between nucleo-  
916 somes have much stronger influence on chromatin  
917 arrays with medium linkers, characterized by  $i \pm 2$

918 and  $i \pm 5$  interactions, compared to very short (NRL =  
919 173 bp or less) or long (NRL = 218 bp or longer)  
920 linkers. Our interaction-intensity averages indicate  
921 that, in short linker arrays with LH, a tail modifica-  
922 tion will likely affect only its nearest neighbors. In  
923 contrast, a tail modification in a highly compacted  
924 chromatin fiber with medium-length linkers could  
925 affect multiple nonadjacent nucleosomes. This sce-  
926 nario might explain the versatility of the epigenetic  
927 control in higher organism.

## 928 Computational Methods

### 929 Model overview

930 Our multiscale mesoscopic model was recently  
931 detailed in a study of the role of histone tails<sup>45</sup> along  
932 with a summary of prior validation studies.<sup>24,42,43</sup> In  
933 the sections below, we present the main features of  
934 the model, including modeling of chromatin's  
935 structural elements, treatment of ionic screening,  
936 details of energy terms, and validation of model. We  
937 also summarize the MC conformational sampling  
938 algorithm, chromatin simulation program, and data  
939 analysis tools.

940 The mesoscopic model incorporates all key struc-  
941 tural elements of chromatin represented at various  
942 levels of accuracy (see Fig. 1) using different  
943 modeling strategies: the nucleosome core with  
944 wrapped DNA excluding protruding tails is repre-  
945 sented as an electrostatic object by Debye-Hückel  
946 charges;<sup>41,74,75</sup> the DNA linker is represented by  
947 beads in the worm-like chain model;<sup>47,76</sup> and the  
948 histone tails and LH are coarse grained as beads.<sup>45</sup>  
949 The geometry of the basic chromatin unit is derived  
950 from available structural data.<sup>29</sup> Despite inherent  
951 limitations of the coarse-grained approach, the  
952 combined model matches the experimentally mea-  
953 sured sedimentation and diffusion coefficients,  
954 linear mass values, and other experimental mea-  
955 surements of static and dynamic properties.<sup>42-46</sup>  
956 Here, we systematically probe chromatin fiber  
957 configurations at linker lengths relevant to biology  
958 (26 to 79 bp) with 24-nucleosome arrays. We have  
959 also performed simulations for 48-core arrays for  
960 illustrative purposes.

### 961 Nucleosome core model

962 Our oligonucleosome chain contains  $N_C$  nucleo-  
963 some cores. Each nucleosome represents the four  
964 histone dimers without protruding tails and the 147  
965 DNA base pairs tightly wound 1.75 times around  
966 them, as an electrostatically charged object (Fig. 1).  
967 Specifically, 300 charges are evenly distributed over  
968 the nonuniform surface based on the nucleosome  
969 crystal structure (Protein Data Bank code: 1KX5).<sup>29</sup>

The irregular discrete charge optimization (DiSCO) 970  
algorithm<sup>41</sup> is used to define the values of those 971  
charges through a Debye-Hückel approximation of 972  
the electric field by an optimization procedure that 973  
minimizes the error between the Debye-Hückel 974  
approximation and the electric field of the full 975  
atom representation of the nucleosome core (more 976  
than 13,000 atoms) at distances  $>5$  Å. The 977  
optimization is achieved through the truncated 978  
Newton TNPack optimization routine,<sup>77-79</sup> inte- 979  
grated within the DiSCO package, as described by 980  
Beard and Schlick<sup>75</sup> and Zhang *et al.*<sup>41</sup> The electric 981  
field is computed using the nonlinear Poisson- 982  
Boltzmann equation (PBE) solver QNIFFT 1.2.<sup>80-82</sup> 983  
The atomic radii input for QNIFFT is taken from 984  
the default extended atomic radii based loosely on 985  
M. Connolly's Molecular Surface program,<sup>83</sup> and 986  
the charges are taken from the AMBER 1995 force 987  
field.<sup>84</sup> Representative charges and positions of 988  
the 300 pseudocharges within the nucleosome are 989  
given in Supplemental Table S1 for the monova- 990  
lent ion concentration  $C_S = 0.15$  M. Data for other 991  
salt concentrations are available from the authors 992  
upon request. The excluded volume of the whole 993  
nucleosome is treated through the effective 994  
excluded volumes of each charge by a Lennard- 995  
Jones potential (Supplemental Table S2). 996

### DNA linker model and the oligonucleosome chain 997

Each nucleosome core, other than the first core, is 998  
attached to (is 'parent of') two DNA linkers (the 999  
'exiting' and 'entering' linker DNA). The double- 1000  
stranded DNA linker connecting two adjacent 1001  
nucleosome cores is modeled as an elastic worm- 1002  
like chain of  $n_b$  discrete spherical beads.<sup>47,76</sup> Each 1003  
inter-bead segment has an equilibrium length ( $l_0$ ) of 1004  
3 nm, and each bead carries a salt-concentration- 1005  
dependent negative charge assigned through Stig- 1006  
ter's procedure developed on the basis of the charged 1007  
rod approximation.<sup>85</sup> The resulting DNA bead 1008  
charges at monovalent salt concentrations of 0.01, 1009  
0.15, and 0.2 M are  $-7.54e$ ,  $-24.09e$ , and  $-29.77e$ , 1010  
respectively. 1011

The sequence of  $N_C$  nucleosomes and  $n_b$  DNA 1012  
beads forms the oligonucleosome chain, starting 1013  
from  $i=1$  for the first nucleosome to  $i=N$  1014  
( $N = N_C(n_b + 1)$ ) for the last linker DNA bead, as 1015  
illustrated in Supplemental Fig. S7a. Consistent 1016  
with the crystal structure, the points of attachment 1017  
of the exiting and entering linker DNA to the 1018  
nucleosome define an angle  $\theta_0$  about the center of 1019  
the nucleosome core and are separated by a 1020  
distance  $2\omega_0$  normal to the plane of the nucleosome 1021  
core (see Supplemental Table S2 and Supplemental 1022  
Fig. S7b and c). Each bead is assigned an excluded 1023  
volume through the Lennard-Jones potential to 1024  
prevent a possible overlap between DNA beads 1025  
and other components of the chromatin array 1026



(Supplemental Table S2). This approach significantly reduces the number of degrees of freedom (from around 800 atoms to approximately 1 bead per DNA twist). The dynamics of DNA chains are governed by the internal force field comprising of stretching, bending, and twisting energy terms as described in Ref. 45 (see energy function in Chromatin energy function).

Within the oligonucleosome chain, each linker DNA bead and nucleosome is allowed to twist about the DNA axis. This is implemented by assigning local coordinate systems to all DNA linker beads and nucleosome cores. As detailed in Supplemental Fig. S7, the coordinate system of each chain component  $i$  is specified by three orthonormal unit vectors  $\{\mathbf{a}_i, \mathbf{b}_i, \mathbf{c}_i\}$ , where  $\mathbf{c}_i = \mathbf{a}_i \times \mathbf{b}_i$ . For each nucleosome core  $i$ , three additional coordinate systems are defined to describe the DNA bending and twisting at their points of attachment to the nucleosome:  $\{\mathbf{a}_i^{\text{DNA}}, \mathbf{b}_i^{\text{DNA}}, \mathbf{c}_i^{\text{DNA}}\}$  represents the direction from the attachment point of the exiting linker DNA to the center of the  $i+1$  DNA bead;  $\{\mathbf{a}_i^+, \mathbf{b}_i^+, \mathbf{c}_i^+\}$  represents the local tangent on the nucleosome core at the point of attachment of the exiting linker DNA; and  $\{\mathbf{a}_i^-, \mathbf{b}_i^-, \mathbf{c}_i^-\}$  represents the tangent corresponding to the entering linker DNA.

To transform the coordinate system of one linker DNA to that of the next (or to that of the entering point of attachment to the core) along the oligonucleosome chain (i.e.,  $\{\mathbf{a}_i, \mathbf{b}_i, \mathbf{c}_i\} \rightarrow \{\mathbf{a}_{i+1}, \mathbf{b}_{i+1}, \mathbf{c}_{i+1}\}$ ), we define the Euler angles  $\alpha_i, \beta_i,$  and  $\gamma_i$  as follows:

$$\beta_i = \cos^{-1}(\mathbf{a}_i \cdot \mathbf{a}_{i+1}) \quad (1)$$

1058

$$\alpha_i = \begin{cases} \cos^{-1}\left(\frac{\mathbf{a}_i \cdot \mathbf{a}_{i+1}}{\sin(\beta_i)}\right) & \text{if } \mathbf{a}_{i+1} \cdot \mathbf{c}_i > 0 \\ -\cos^{-1}\left(\frac{\mathbf{a}_i \cdot \mathbf{a}_{i+1}}{\sin(\beta_i)}\right) & \text{if } \mathbf{a}_{i+1} \cdot \mathbf{c}_i < 0 \end{cases} \quad (2)$$

1060 and

$$\gamma_i = \begin{cases} \cos^{-1}\left(\frac{\mathbf{b}_i \cdot \mathbf{b}_{i+1} + \mathbf{c}_i \cdot \mathbf{c}_{i+1}}{1 + \mathbf{a}_i \cdot \mathbf{a}_{i+1}}\right) - \alpha_i & \text{if } \frac{\mathbf{c}_i \cdot \mathbf{b}_{i+1} + \mathbf{b}_i \cdot \mathbf{c}_{i+1}}{1 + \mathbf{a}_i \cdot \mathbf{a}_{i+1}} > 0 \\ -\cos^{-1}\left(\frac{\mathbf{b}_i \cdot \mathbf{b}_{i+1} + \mathbf{c}_i \cdot \mathbf{c}_{i+1}}{1 + \mathbf{a}_i \cdot \mathbf{a}_{i+1}}\right) - \alpha_i & \text{if } \frac{\mathbf{c}_i \cdot \mathbf{b}_{i+1} + \mathbf{b}_i \cdot \mathbf{c}_{i+1}}{1 + \mathbf{a}_i \cdot \mathbf{a}_{i+1}} < 0 \end{cases} \quad (3)$$

The Euler angles  $\alpha_i^+, \alpha_i^-,$  and  $\gamma_i^+$  are defined equivalently and transform the coordinate system of the nucleosome core to that of the exiting linker DNA (i.e.,  $\{\mathbf{a}_i, \mathbf{b}_i, \mathbf{c}_i\} \rightarrow \{\mathbf{a}_i^{\text{DNA}}, \mathbf{b}_i^{\text{DNA}}, \mathbf{c}_i^{\text{DNA}}\}$ ). Further details on the Euler angles and a geometric description of the oligonucleosome chain are provided in Ref. 42, 45, and 75 and the supplementary material of Ref. 74.

The 3-nm equilibrium length of each DNA inter-bead segment in our chromatin model determines the values of the NRL that we can model. For a given number of inter-bead segments,  $n_s = n_b + 1$ , the linker length measured in base pairs is simply computed as  $l_{n_s}^{\text{DNA}} = n_s l_0 / a$ , where  $a = 0.34$  nm/bp is the rise per base pair. Thus, for 3 to 9 bead segments, the linker lengths  $l_{n_s}^{\text{DNA}}$  are 26.47, 35.29, 44.12, 52.94, 61.76, 70.59, and 79.41 bp (Table 2). Since the NRL is defined as the linker length plus the 147 bp of DNA wound around the nucleosome core, the DNA linker lengths we can model are closest to integer NRL of 173, 182, 191, 200, 209, 218, and 226 bp. The shortest theoretical DNA linker length of two segments (one DNA bead) was not considered because it is too short for the worm-like chain model. NRL longer than 226 bp were also not considered because they rarely occur in nature.

To implement the correct non-integral twist for each DNA segment, we first estimate the actual number of turns,  $\tau_{n_s}$ , that each DNA linker should make according to its length by dividing the linker length over the number of base pairs per turn for DNA in chromatin ( $l_r$ ); that is,  $\tau_{n_s} = l_{n_s}^{\text{DNA}} / l_r$ . Here, we use  $l_r = 10.3$  bp/turn for DNA in chromatin, based on experimental observations.<sup>86,87</sup> Note that a range of 10.2–10.5 bp/turn has been reported for DNA of chromatin, which is different from the twist for nucleosome-free DNA. The resulting  $\tau_{n_s}$  values in Table 2 are non-integral for all the NRL studied, except for NRL = 209 bp, where the linker length corresponds to six full helical turns. When the length of the linker DNA corresponds to an integral number of turns, the average mean twist of that DNA section is exactly zero. However, a non-integral number of turns shifts the average twist of the DNA linker involved.

Thus, to model the different DNA linker lengths, we incorporate the appropriate equilibrium twist per DNA linker segment to accommodate non-integral numbers of DNA turns. In practice, we accomplish this by including a penalty term in the total torsional energy of the bead segments. This torsional energy is

$$E_T = \frac{s}{2l_0} \sum_{i=1}^{N-1} (\alpha_i + \gamma_i - \varphi_{n_s})^2 \quad (4)$$

where  $s$  is the torsional rigidity of DNA,  $N$  is the number of beads in the oligonucleosome chain,  $\varphi_{n_s}$  is the twist deviation penalty term per segment, and  $\alpha_i$  and  $\gamma_i$  are two of the Euler angles defined above. The sum  $\alpha_i + \gamma_i \in [-\pi, \pi]$  gives the linker DNA twist at each bead location. Thus, subtracting  $\varphi_{n_s}$  from this sum of angles shifts the average linker DNA twist per segment from zero to the required value.

The values of the twist penalty term per segment are obtained as follows: first, the difference between

the required number of turns for the DNA linker and an integral number of turns is calculated (e.g.,  $\text{int}(\tau_{n_s}) - \tau_{n_s}$ ); second, the obtained fractional number of turns is converted into radians  $\in [-\pi, \pi]$ ; finally, the resulting twist deviation of the DNA linker is divided by  $n_s$  to obtain the twist deviation per segment. Given that the sign of  $\varphi_{n_s}$  only affects the direction of the relative rotation between consecutive DNA beads, both  $+\varphi_{n_s}$  and  $-\varphi_{n_s}$  produce the same behavior in our simulations. In other words, the fractional number of turns can be computed as a difference from the higher or lower integer turn value. For example, our shortest DNA linker of 173 bp NRL is modeled by two beads or three inter-bead segments, which corresponds to an actual linker length of  $l_3^{\text{DNA}} = (9 \text{ nm}) / (0.34 \text{ nm/bp}) = 26.47 \text{ bp}$  and  $\tau_3 = (26.47 \text{ bp}) / (10.3 \text{ bp/turn}) = 2.57$  helical turns around the DNA axis. The difference from 2 or 3 turns ( $-0.57$  or  $+0.43$ ) yields the same twist deviation of 2.7 rad for a whole linker DNA and a penalty term per DNA segment of  $\varphi_{n_s} = 2.7 / n_s = 0.9$  rad. For consistency, in Table 2, we define the difference as the lower integer minus the actual number of turns.

#### Flexible histone tail model

There are 10 histone tails per nucleosome core: tails belonging to N-termini of H2A (denoted H2A<sub>1</sub>), H2B, H3, and H4 histones, plus C-termini tails of H2A histones (denoted as H2A<sub>2</sub>). The histone tails are modeled as chains of spherical beads with each bead representing five adjacent amino acids.<sup>88,42,43</sup> Each of the two H2A<sub>1</sub>, H2A<sub>2</sub>, H2B, H3, and H4 histone tails is represented using 4, 3, 5, 8, and 5 beads, respectively, for a total of 50 tail beads per nucleosome to model the 250 or so histone tail residues that comprise each nucleosome. The lengths of the H2A<sub>1</sub>, H2A<sub>2</sub>, H2B, H3, and H4 tails are 6.2, 4.7, 7.8, 12.6, and 7.8 nm, respectively.

Each histone tail is rigidly fixed to its idealized position in the nucleosome crystal structure by a stiff spring between the core and the first tail bead (Fig. 1). For tail beads not attached to the core, the stretching and bending harmonic potentials between beads and bond angles between three consecutive beads are tuned to reproduce configurational properties of the atomistic histone tails obtained via Brownian dynamics simulations;<sup>42,88</sup> the derived force constants are given in Supplemental Tables S3 and S4. The excluded volume of each tail bead is modeled through a Lennard-Jones potential with fixed parameters  $k_{\text{ev}}$  and  $\sigma_{\text{tt}}$  (Supplemental Table S2).

The electrostatic interactions of histone tails in the presence of salt are modeled by rescaling the charges to reproduce the atomistic potential. For salt concentrations of 0.01, 0.15, and 0.2 M, the scaling factors for the bead charges are 0.75, 1.12, and 1.2.

The tails interact with all of the chromatin components, except for the few components listed below, by means of excluded volume and electrostatic interactions. The interactions between neighboring tail beads belonging to the same chain do not interact electrostatically with each other as their interactions are already accounted for through the intramolecular force field. To ensure that the tail bead attachment remains as close as possible to the equilibrium location, we made sure that histone tail beads directly attached to the nucleosome do not interact with the nucleosome pseudocharges.<sup>45</sup>

#### LH model

The rat H1d LH was the basis for the LH model.<sup>46</sup> Its structure was predicted through fold recognition and molecular modeling.<sup>49,89</sup> H1d is made of three domains, an N-terminal region of 33 residues, a central globular domain of 76 residues, and a highly charged C-terminal domain of 110 residues. In our model, we neglected the short, relatively uncharged N-terminal region and interpret only central globular and C-terminal domains. We model the C-terminal domain by two charged beads and globular domain by a single bead. The three beads are rigidly fixed for each nucleosome and placed on the dyad axis separated by a distance of 2.6 nm.<sup>49,89,90</sup>

The DiSCO approximation developed for the nucleosome core modeling<sup>74</sup> was applied to assign charges to each linker bead as well.<sup>46</sup> The Debye-Hückel potential of a coarse-grained model of each domain (globular and C-terminal) was fitted to the full atom electrostatic potentials obtained by solving the complete nonlinear PBE. Consequently, the globular bead carries an effective charge of  $+13.88e$  and each C-terminal bead carries a charge of  $+25.62e$  at 0.15 M salt. The LH also interacts electrostatically with the other chromatin components except for the nucleosome charges and non-parental DNA linkers. Unlike histone tails or DNA, the three LH beads hold fixed relative positions with respect to each other and their parent cores, making the core and LH a unified object that moves as a whole. Compatible with this ‘unified core-linker-histone object’, interactions between LHs and core charges and between non-parent DNA linker and LH are excluded.

Apart from electrostatic interactions, each LH bead interacts with all chromatin components except their parent nucleosome through a Lennard-Jones excluded volume potential.

#### Chromatin interaction energies

Below, we summarize our treatment of chromatin electrostatics with monovalent and divalent ions, followed by energy terms for interactions among chromatin constituents.

### 1238 *Chromatin electrostatics with monovalent and* 1239 *divalent ions*

1240 Physiological salt conditions with monovalent and  
1241 divalent cations are indispensable for compacting  
1242 chromatin by screening the highly charged chromatin  
1243 components (e.g., nucleosomal and linker DNA). We  
1244 treat the counterions implicitly using mean field  
1245 theories. Specifically, our DiSCO algorithm<sup>41,75</sup> para-  
1246 meterizes the screening potential from the PBE using  
1247 a Debye–Hückel approximation with salt-dependent  
1248 effective charges, obtained by minimizing the differ-  
1249 ence between the electric fields from PBE and the  
1250 (linear) Debye–Hückel approximation using our  
1251 efficient TNPACK (truncated Newton) optimization  
1252 package.<sup>77,78</sup> Thus, DiSCO is used to evaluate the  
1253 effective charges on the nucleosome core, LHs, and  
1254 histone tails; the effective charges for DNA beads are  
1255 obtained using an analytical method by Stigter.<sup>85</sup> For  
1256 the nucleosome core, we typically use 300 effective  
1257 charges uniformly distributed across the nucleosome  
1258 surface; this produces a robust approximation, with  
1259 <10% error in the DH approximation over a large  
1260 range of salt concentrations.<sup>41,75</sup>

1261 The DiSCO approach has been implemented for  
1262 monovalent ions and assumes that the screening  
1263 potential is independent of chromatin conformation.  
1264 To treat divalent ions, we developed a first-order  
1265 approximation following experimental studies on  
1266 DNA bending,<sup>91,92</sup> which suggest a reduction of the  
1267 DNA persistence length to promote linker bending.  
1268 Specifically, we reduce the repulsion among linker  
1269 DNA in linker/linker interactions by setting an  
1270 inverse Debye length of 2.5 nm<sup>-1</sup> to allow DNA to  
1271 almost touch one another and reduce the persistence  
1272 length of the linker DNA sequences from 50 to  
1273 30 nm according to experimental findings.<sup>91,92</sup> A  
1274 refinement of this simple approach has recently been  
1275 developed.<sup>93</sup>

### 1276 *Chromatin energy function*

1277 The total potential energy is expressed as the sum  
1278 of stretching, bending, and torsional components of  
1279 linker DNA, stretching of histone tails, intramolec-  
1280 ular bending of the histone tails, total electrostatic  
1281 energy, and excluded volume terms:<sup>42</sup>

$$E = E_S + E_B + E_T + E_{tS} + E_{tB} + E_C + E_V \quad (5)$$

1283 The first three terms denote stretching,

$$E_S = \frac{h}{2} \sum_{i=1}^{N-1} (l_i - l_0)^2 \quad (6)$$

1285 bending,

$$E_B = \frac{g}{2} \left[ \sum_{i=1}^N (\beta_i)^2 + \sum_{i \in I_C} (\beta_i^+)^2 \right] \quad (7)$$

and torsional energy of the linker DNA [Eq. (4)].<sup>1286</sup>  
Here,  $h$  and  $g$  denote the stretching and bending  
1288 rigidities of DNA,  $l_i$  denotes the separation between  
1289 the DNA beads, and  $I_C$  denotes a nucleosome  
1290 particle within the oligonucleosome chain (see  
1291 parameters in [Supplemental Table S2](#)). As men-  
1292 tioned above,  $N$  is the total number of beads in the  
1293 chromatin chain,  $\beta_i$  and  $\beta_i^+$  are bending angles, and  
1294  $l_0$  is the equilibrium separation distance between  
1295 beads of relaxed DNA.<sup>1296</sup>

The fourth term,  $E_{tS}$ , represents the total stretching  
1297 energy of the histone tails, composed of two terms:  
1298 stretching of tail beads and stretching of the histone  
1299 tail bead from its assigned attachment site, as given  
1300 by:<sup>1301</sup>

$$E_{tS} = \sum_{i \in I_C}^N \sum_{j=1}^{N_T} \sum_{k=1}^{N_{bj}-1} \frac{k_{b_{jk}}}{2} (l_{ijk} - l_{jk0})^2 \quad (8)$$

$$+ \frac{h_{tc}}{2} \sum_{i \in I_C}^N \sum_{j=1}^{N_T} |\mathbf{t}_{ij} - \mathbf{t}_{j0}|^2$$

Here,  $N_T = 10N_C$  is the total number of histone tails,<sup>1302</sup>  
 $N_{bj}$  is the number of beads in the  $j$ th tail,  $k_{b_{jk}}$  is  
1304 the stretching constant of the bond between the  
1305  $k$ th and  $(k+1)$ th beads of the  $j$ th histone tail, and  $l_{ijk}$   
1306 and  $l_{jk0}$  represent the distance between tail beads  $k$   
1307 and  $k+1$  and their equilibrium separation distance,  
1308 respectively. In the second term,  $h_{tc}$  is the stretching  
1309 bond constant of the spring attaching the histone tail  
1310 to the nucleosome core,  $\mathbf{t}_{ij}$  is the position vector of  
1311 the first tail bead in the coordinate system of its  
1312 parent nucleosome, and  $\mathbf{t}_{j0}$  is the ideal position  
1313 vector in the crystal configuration.<sup>1314</sup>

The fifth term,  $E_{tB}$ , represents the intramolecular  
1315 bending contribution to the histone tail energies:<sup>1316</sup>

$$E_{tB} = \sum_{i \in I_C}^N \sum_{j=1}^{N_T} \sum_{k=1}^{N_{bj}-2} \frac{k_{\theta_{jk}}}{2} (\theta_{ijk} - \theta_{jk0})^2 \quad (9)$$

where  $\theta_{ijk}$  and  $\theta_{j0}$  represent the angle between three  
1318 consecutive tail beads ( $k$ ,  $k+1$ , and  $k+2$ ) and their  
1319 equilibrium angle, respectively, and  $k_{\theta_{jk}}$  is the  
1320 corresponding bending force constant. The sixth  
1321 term,  $E_C$ , represents the total electrostatic interaction  
1322 energy of the oligonucleosome. All these interac-  
1323 tions are modeled using the Debye–Hückel potential  
1324 that accounts for salt screening:<sup>1325</sup>

$$E_C = \sum_i \sum_{j \neq i} \frac{q_i q_j}{4\pi\epsilon\epsilon_0 r_{ij}} \exp(-\kappa r_{ij}) \quad (10)$$

where  $q_i$  and  $q_j$  are the ‘effective’ charges separated  
1326 by a distance  $r_{ij}$  in a medium with a dielectric  
1327 constant of  $\kappa$  and an inverse Debye length of  $1/\kappa$ ,  $\epsilon_0$   
1328 is the electric permittivity of vacuum, and  $\epsilon$  is the  
1329 dielectric constant (set to 80). As described above,  
1330 the salt-dependent effective charges are calculated  
1332

1333 using DiSCO<sup>41,75</sup> by matching the electric field from  
 1334 the PBE (solved using the DelPhi software) to the  
 1335 field parameterized using the Debye–Hückel form  
 1336 [see Eq. (10)].

1337 The last term,  $E_V$ , represents the total excluded  
 1338 volume interaction energy of the oligonucleosome.  
 1339 The excluded volume interactions are modeled  
 1340 using the Lennard–Jones potential, and the total  
 1341 energy is given by:

$$E_V = \sum_i \sum_{j \neq i} k_{ij} \left[ \left( \frac{\sigma_{ij}}{r_{ij}} \right)^{12} - \left( \frac{\sigma_{ij}}{r_{ij}} \right)^6 \right] \quad (11)$$

1342 where  $\sigma_{ij}$  is the effective diameter of the two  
 1343 interacting beads and  $k_{ij}$  is an energy parameter  
 1344 that controls the steepness of the excluded volume  
 1345 potential. These parameters were all taken from  
 1346 relevant models of the components as described  
 1347 fully and tabulated in Supplemental Tables S2–S4  
 1348 and Ref. 45.

### 1350 MC sampling algorithm and model validation

1351 Sampling of the chromatin configurations is  
 1352 performed by MC simulations as developed  
 1353 previously.<sup>42–44</sup> We employ four different MC  
 1354 moves (pivot, translation, rotation, and tail re-  
 1355 growth) to efficiently sample from the ensemble of  
 1356 oligonucleosome conformations at constant temper-  
 1357 ature. Global pivot moves are implemented by  
 1358 randomly choosing one of the linker beads or  
 1359 nucleosome cores, selecting a random axis passing  
 1360 through the chosen component, and then rotating  
 1361 the shorter part of the oligonucleosome about this  
 1362 axis by an angle chosen from a uniform distribution  
 1363 within [0,20]. Local translation and rotation moves  
 1364 also begin by choosing a randomly oriented axis  
 1365 passing through randomly picked linker bead  
 1366 nucleosome core. In a translation move, the chosen  
 1367 component is shifted along the axis by a distance  
 1368 sampled from a uniform distribution in the range  
 1369 [0,0.6 nm], whereas in a rotation move, it is rotated  
 1370 about the axis by an angle uniformly sampled from  
 1371 the range [0,36]. All three MC moves are accepted/  
 1372 rejected based on the standard Metropolis criterion.  
 1373 The tail regrowth move is implemented to enhance  
 1374 sampling of histone tail conformations. This move  
 1375 employs the configurational bias MC method<sup>94,95</sup> to  
 1376 randomly select a histone tail chain and regrow it on  
 1377 the other end using the Rosenbluth scheme.<sup>96</sup> The  
 1378 volume enclosed within the nucleosomal surface is  
 1379 discretized to prevent histone tail beads from  
 1380 penetrating the nucleosome core during tail re-  
 1381 growth, and any insertion attempts that place the  
 1382 tail beads within this volume are rejected automat-  
 1383 ically. Typically, the pivot, translation, rotation, and  
 1384 tail regrowth moves are attempted with probabili-  
 1385 ties of 0.2, 0.1, 0.1, and 0.6, respectively.<sup>42,43</sup>

Our mesoscale chromatin simulation program has  
 been validated for many experimentally measured  
 properties (see Refs. 24, 42, 43, and 45). These  
 properties include salt-induced compaction of oli-  
 gonucleosomes to reproduce experimental sedimen-  
 tation coefficients<sup>55</sup> and nucleosome packing  
 ratios;<sup>7,97,98</sup> diffusion and salt-dependent behavior  
 of mononucleosomes, dinucleosomes, and  
 trinucleosomes;<sup>99,100,101</sup> salt-dependent extension  
 of histone tails measured via the tail-to-tail diameter  
 of the core and radius of gyration for mononucleo-  
 somes over a broad range of monovalent salt  
 concentrations;<sup>102</sup> the irregular zigzag topology of  
 chromatin fibers consistent with experimental  
 models<sup>7,30,101,103</sup> and its enhanced compaction  
 upon LH binding;<sup>30</sup> linker crossing orientations in  
 agreement with various experiments;<sup>7,104–106</sup> and  
 internucleosome interaction patterns consistent with  
 cross-linking and EM experiments.<sup>46</sup> Importantly,  
 the refined model with tails improved the agree-  
 ment with experimental results compared to the  
 rigid-tail model.<sup>45</sup>

### Data collection

We conducted MC sampling with variable linker  
 lengths with 24 nucleosome arrays. Every experi-  
 mental set (number of nucleosomes, DNA linker  
 length, LH presence) includes a set of 24 simula-  
 tions divided into two groups according to the  
 starting configuration, zigzag, and interdigitated  
 solenoid. Each group covers the mean DNA twist  
 angle (Table 2) and two DNA twist deviations,  
 $-12^\circ$ , and  $+12^\circ$  from the mean twist to mimic  
 natural variations, by four independent MC trajec-  
 tories. The additional DNA twist variations ac-  
 count for natural variations. We conducted  
 experiments with and without LH. Additionally,  
 we conducted simulations with 48 cores for  
 visualization purposes. The starting configurations  
 for 48-core oligonucleosomes were generated from  
 the compacted 24-core oligonucleosomes. The bulk  
 of our simulations were performed under identical  
 experimental conditions: temperature of 293.15 K  
 and 0.15 M monovalent salt concentration ( $C_S$ ). To  
 analyze salt effects, for selected NRL, three  
 additional experimental sets were assayed (via 24  
 trajectories each): low monovalent salt ( $C_S=0.01$  M)  
 without LH, high monovalent salt ( $C_S=0.2$  M) with  
 LH, and moderate monovalent salt ( $C_S=0.15$  M)  
 with divalent ions and LH. Each simulation  
 trajectory was 35 to 50 million MC steps long.  
 The last 5 million steps were used for statistical  
 analysis. Simulations were run on a 2.33-GHz Intel-  
 Xeon machine. Typically, a 10-million step simula-  
 tion of 24-core oligonucleosomes takes 4–6 CPU  
 days. Convergence was monitored by global and  
 local geometric and energetic terms (Supplemental  
 Fig. S2).

1443 **Calculation of interaction patterns**1444 *Internucleosome interactions*

1445 The internucleosome interactions matrices  $I'(i,j)$   
 1446 describe the fraction of MC iterations that cores  $i$   
 1447 and  $j$  are in contact with one another. Each matrix  
 1448 element is defined as:

$$I'(i,j) = \text{mean}[\delta_{i,j}(M)], \quad (12)$$

1449 where  $M$  is the MC configurational frame, and the  
 1451 mean is calculated over converged MC frames used  
 1452 for statistical analysis where

$$\delta_{i,j}(M) = \begin{cases} 1 & \text{if cores } i \text{ and } j \text{ are 'in contact' \\ & \text{at MC frame } M, \\ 0 & \text{otherwise} \end{cases} \quad (13)$$

1453 At a given MC step  $M$ , we consider nucleosomes  $i$   
 1455 and  $j$  to be in contact if the shortest distance  
 1456 between the tail beads directly attached to  $i$  and the  
 1457 tail beads or core charges of core  $j$  is smaller than the  
 1458 tail-tail ( $\sigma_{tt}$ ) or tail-core ( $\sigma_{tc}$ ) excluded volume  
 1459 distance, respectively.<sup>42</sup> In our computations, we  
 1460 use this cutoff value of 1.8 nm. [Supplemental Fig. S3](#)  
 1461 shows a typical two-dimensional map [ $I'(i,j)$ ] of the  
 1462 frequency of histone-tail-mediated interactions for a  
 1463 zigzag fiber.

1464 These matrices can be projected into normalized  
 1465 one-dimensional maps

$$I(k) = \frac{\sum_{i=1}^{N_C} I'(i, i \pm k)}{\sum_{j=1}^{N_C} I(j)} \quad (14)$$

1466 that depict the relative intensity of interactions  
 1468 between cores separated by  $k$  neighbors. These maps  
 1469 reveal the pattern of internucleosome interactions  
 1470 (dominant, moderate, weak) in a chromatin fiber,  
 1471 providing key insights into structural organization.

1472 *Tail interactions*

1473 To calculate the interactions of tails with different  
 1474 nucleosome components, we follow a similar  
 1475 procedure to that described above. Namely, we  
 1476 measure the fraction of the time that tails of a  
 1477 specific kind  $t$  ( $t = \text{H2A}_1, \text{H2A}_2, \text{H2B}, \text{H3}, \text{and H4}$ ) in  
 1478 a chromatin chain are 'in contact' with a specific  
 1479 component  $c$  of the chromatin chain ( $c = \text{its parent}$   
 1480 nucleosome, a non-parental nucleosome, parent  
 1481 DNA linkers, or non-parental DNA linkers) by  
 1482 constructing two-dimensional matrices with the  
 1483 following elements

$$T'(t,c) = \text{mean} \left[ \frac{1}{N_C N} \sum_{i \in c} \sum_{j=1}^N \delta_{i,j}^{t,c}(M) \right] \quad (15)$$

with the average taken over the converged MC 1483  
 configurations used for statistical analysis with 1486

$$\delta_{i,j}^{t,c}(M) = \begin{cases} 1 & \text{if } j \text{ is a } c\text{-type component 'in contact'} \\ & \text{with tail of kind } t \text{ of nucleosome} \\ & i \text{ at frame } M \\ 0 & \text{otherwise} \end{cases} \quad (16)$$

For a given frame  $M$ , we consider a specific  $t$ -kind 1488  
 tail of core  $i$  to be either free or in contact with only 1490  
 one of the  $N$  chromatin components of the oligonu- 1491  
 cleosome chain. The  $t$ -tail is in contact with a 1492  
 component of type  $c$  if the shortest distance between 1493  
 its beads and the beads or core charges of  $c$  is smaller 1494  
 than the shortest distance to any other type of 1495  
 component and also smaller than the relevant tail- 1496  
 component excluded volume distance ([Supplemen- 1497](#)  
[ental Table S2](#)). The resulting normalized patterns of 1498  
 interactions provide crucial information into the 1499  
 frequency by which different tails mediate chroma- 1500  
 tin interactions. 1501

1502 **Bending, triplet, and dihedral angles**

The local bending angle between consecutive 1503  
 nucleosomes is defined as in Ref. 45 as the angle 1504  
 formed between the vector exiting one nucleosome 1505  
 and the vector entering the next nucleosome. The 1506  
 former connects the centers of the first two linker 1507  
 DNA beads and the latter connects those of the last 1508  
 two linker DNA beads ([Supplemental Fig. S4](#)). 1509

The local triplet angle for three consecutive 1510  
 nucleosomes is the angle defined by nucleosome 1511  
 centers  $\{i, j+1, i+2\}$ . 1512

The local dihedral angle is defined for four 1513  
 consecutive nucleosome centers  $\{i, j+1, i+2, i+3\}$  1514  
 (see [Supplemental Fig. S4](#)). 1515

For a given MC frame, we calculate the bending, 1516  
 triplet, and dihedral angles of a fiber by taking the 1517  
 average of the local angles over all the nucleosome 1518  
 pairs, triplets, or quadruplets, respectively. We then 1519  
 repeat this procedure for each simulation frame and 1520  
 average the values to obtain mean bending, triplet, 1521  
 and dihedral angles. 1522

1523 **Calculation of sedimentation coefficients**

We applied the method developed by Bloomfield 1524  
*et al.*<sup>107,108</sup> to calculate the sedimentation coefficient 1525  
 of a given oligonucleosome array conformation, 1526  
 from the inter-core distances.<sup>55,109</sup> The sedimentation 1527  
 coefficient  $S_{20,w}$  is approximated from  $S_{N_C}$ , where 1528

$$\frac{S_{N_C}}{S_1} = 1 + \frac{R_1}{N_C} \sum_i \sum_j \frac{1}{R_{ij}} \quad (17)$$

Here,  $S_{N_C}$  represents  $S_{20,w}$  for a rigid structure 1529  
 consisting of  $N_C$  nucleosomes of radius  $R_1$ ,  $R_{ij}$  is the 1531  
 distance between the centers of two nucleosomes, 1532

and  $S_1$  is  $S_{20,w}$  for a mononucleosome. This approach assumes spherical nucleosomes, a reasonable approximation. We use  $R_1=5.5$  nm and  $S_1=11.1$  Svedberg ( $1\text{ S}=10^{-13}$  s) as done previously.<sup>109</sup> Similar results can be obtained by a more complex procedure implemented in the program HYDRO,<sup>110</sup> which calculates  $S_{20,w}$  using the radii of both the nucleosome core particle (5.0 nm) and the DNA bead (1.5 nm).

### 1542 Calculation of fiber packing ratio, curvature, and 1543 volume

1544 To calculate the fiber packing ratio (number of  
1545 nucleosomes per 11 nm of fiber length) for each  
1546 simulation frame, we first compute the length of the  
1547 fiber axis passing through a chromatin fiber core  
1548 (Supplemental Fig. S6). At each simulation frame,  
1549 we define the fiber axis as a three-dimensional  
1550 parametric curve  $\mathbf{r}^{\text{ax}}(i) = (r_1^{\text{ax}}(i), r_2^{\text{ax}}(i), r_3^{\text{ax}}(i))$ , where  
1551  $r_j^{\text{ax}}(i)$  ( $j=1, 2$ , and  $3$ ) are three functions that return  
1552 the center positions of the  $i$ th nucleosome ( $r_{i1}$ ,  $r_{i2}$ ,  
1553 and  $r_{i3}$ ) in the  $x$ ,  $y$ , or  $z$  direction, respectively. We  
1554 approximate these functions with polynomials of the  
1555 form

$$r_j^{\text{ax}}(i) \approx P_j(i) = p_{1,j}i^2 + p_{2,j}i + p_{3,j} \quad (18)$$

1556 by fitting the data sets  $[r_{ij}]$  by a least-squares  
1557 procedure. We have chosen second-order polyno-  
1558 mials to approximate the fiber axis because higher-  
1559 order polynomials tend to produce highly nonlinear  
1560 fiber axis curves with small packing ratios. We  
1561 determine the coefficients of the polynomial  $P_j(i)$  by  
1562 minimizing the sum of the squares of the residuals  $l_j$   
1563

$$l_j = \sum_{i=1}^{N_C} (r_{ij} - P_j(i))^2 \quad (19)$$

1564 which account for the differences between a  
1565 proposed polynomial fit and the observed nucleo-  
1566 some positions. After determining the polynomial  
1567 coefficients, we use Eq. (18) to produce  $N_C$  points  
1568 per spatial dimension and compute the fiber length  
1569  $L_{\text{fiber}}$  as follows:  
1570

$$L_{\text{fiber}} = \sum_{i=1}^{(N_C-1)/2} |\mathbf{r}^{\text{ax}}(2i-1) - \mathbf{r}^{\text{ax}}(2i+1)| \quad (20)$$

1571 where the distances are between every two consec-  
1572 utive nucleosome centers. The packing ratio (number  
1573 of cores per 11 nm) is then calculated as the number  
1574 of cores multiplied by 11 nm/ $L_{\text{fiber}}$ . From the fiber  
1575 axis, we define the local fiber radius for a given  
1576 nucleosome core to be the perpendicular distance  
1577 between a nucleosome core center and its closest  
1578 linear fiber axis segment plus the nucleosome radius  
1579 ( $R_{\text{core}}=5.5$  nm). We then average over all local fiber  
1580

1581 radii in a given fiber to obtain the fiber radius at each  
1582 simulation frame. Finally, we repeat this procedure  
1583 for each simulation frame and average the value to  
1584 obtain a mean fiber radius. The fiber width,  $D_{\text{fiber}}$ , is  
1585 twice that value. Additionally, from the parametric  
1586 definition of the fiber axis, we identify the mean  
1587 curvature of the chromatin fiber at each simulation  
1588 frame as:

$$\kappa_{\text{fiber}} = \frac{1}{N_C} \sum_{i=1}^{N_C} \frac{\dot{\mathbf{r}}^{\text{ax}}(i) \times \ddot{\mathbf{r}}^{\text{ax}}(i)}{|\dot{\mathbf{r}}^{\text{ax}}(i)|^3} \quad (21)$$

1589 where  $\dot{\mathbf{r}}^{\text{ax}}(i) \approx (2p_{1,1}i + p_{2,1}, 2p_{1,2}i + p_{2,2}, 2p_{1,3}i + p_{2,3})$ ,  
1590 and  $\ddot{\mathbf{r}}^{\text{ax}}(i) \approx 2(p_{1,1}, p_{1,2}, p_{1,3})$ .

1591 In calculating the fiber volume,  $V_{\text{fiber}}$ , for simplicity,  
1592 we use the fiber length and width described above  
1593 and assume a cylindrical geometry.

1594 We also approximate the percentage of filled  
1595 volume or the volume occupied by the  $N_C$  nucleo-  
1596 somes and linker DNAs divided by the total fiber  
1597 volume. The volume of each nucleosome is approx-  
1598 imated by that of a cylinder with height  $l_{\text{core}}=5.5$  nm  
1599 and radius  $R_1$ . The volume of each linker DNA has  
1600 been approximated as that of a cylinder with  
1601 diameter  $l_0$  and height equal to the segment length  
1602  $l_0$  multiplied by the number of inter-bead segments  
1603  $n_S$  (e.g., for  $NRL=209$  bp,  $n_S=7$  segments or 21 nm  
1604 of height).  
1605

## Acknowledgements

1606 This work was supported by National Science  
1607 Foundation grant MCB-0316771 and National Insti-  
1608 tutes of Health grant R01 GM55164 to T. Schlick.  
1609 Acknowledgment is also made to the donors of the  
1610 American Chemical Society (Award PRF39225-AC4)  
1611 Petroleum Research Fund and Philip Morris USA  
1612 and to Philip Morris International. Computing  
1613 support from the NYU HPC USQ and Cardiac  
1614 clusters is gratefully acknowledged.  
1615

## Supplementary Data

1616 Supplementary data to this article can be found  
1617 online at [doi:10.1016/j.jmb.2010.07.057](https://doi.org/10.1016/j.jmb.2010.07.057)  
1618

## References

- 1619 Luger, K., Mäder, A. W., Richmond, R. K., Sargent,  
1620 D. F. & Richmond, T. J. (1997). Crystal structure of  
1621 the nucleosome core particle at 2.8 Å resolution.  
1622 *Nature*, **389**, 251–260.  
1623
- 1624 Compton, J. L., Bellard, M. & Chambon, P. (1976).  
1625 Biochemical evidence of variability in the DNA

- 1626 repeat length in the chromatin of higher eukaryotes. 1690  
 1627 *Proc. Natl Acad. Sci. USA*, **73**, 4382–4386. 1691
- 1628 3. Woodcock, C. L., Skoultchi, A. I. & Fan, Y. (2006). 1692  
 1629 Role of linker histone in chromatin structure and 1693  
 1630 function: H1 stoichiometry and nucleosome repeat 1694  
 1631 length. *Chromosome Res.* **14**, 17–25. 1695
- 1632 4. Jaeger, A. W. & Kuenzle, C. C. (1982). The chromatin 1696  
 1633 repeat length of brain cortex and cerebellar neurons 1697  
 1634 changes concomitant with terminal differentiation. 1698  
 1635 *EMBO J.* **1**, 811–816. 1699
- 1636 5. Bates, D. L., Jonathan, P., Butler, G., Pearson, E. C. 1700  
 1637 & Thomas, J. O. (1981). Stability of the higher- 1701  
 1638 order structure of chicken-erythrocyte chromatin in 1702  
 1639 solution. *Eur. J. Biochem.* **119**, 469–476. 1703
- 1640 6. Thoma, F., Koller, T. & Klug, A. (1979). Involvement 1704  
 1641 of histone H1 in the organization of the 1705  
 1642 nucleosome and of the salt-dependent superstructures 1706  
 1643 of chromatin. *J. Cell Biol.* **83**, 403–427. 1707
- 1644 7. Bednar, J., Horowitz, R. A., Grigoryev, S. A., 1708  
 1645 Carruthers, L. M., Hansen, J. C., Koster, A. J. & 1709  
 1646 Woodcock, C. L. (1998). Nucleosomes, linker DNA, 1710  
 1647 and linker histone form a unique structural motif 1711  
 1648 that directs the higher-order folding and compaction 1712  
 1649 of chromatin. *Proc. Natl Acad. Sci. USA*, **95**, 1713  
 1650 14173–14178. 1714
- 1651 8. Carruthers, L. M., Bednar, J., Woodcock, C. L. & 1715  
 1652 Hansen, J. C. (1998). Linker histones stabilize the 1716  
 1653 intrinsic salt-dependent folding of nucleosomal 1717  
 1654 arrays: mechanistic ramifications for higher-order 1718  
 1655 chromatin folding. *Biochemistry*, **37**, 14776–14787. 1719
- 1656 9. Spadafora, C., Oudet, P. & Chambon, P. (1979). 1720  
 1657 Rearrangement of chromatin structure induced by 1721  
 1658 increasing ionic strength and temperature. *Eur. J. 1722*  
 1659 *Biochem.* **100**, 225–235. 1723
- 1660 10. Leibovitch, B. A. & Elgin, S. R. (2005). *Encyclopedia of 1724*  
 1661 *Molecular Cell Biology and Molecular Medicine, Chapter 7. 1725*  
 1662 *Heterochromatin and Euchromatin—Organization, 1726*  
 1663 *Packaging, and Gene Regulation*, pp. 137–155, Wiley- 1727  
 1664 VCH, 3527305483. 1728
- 1665 11. Misteli, T., Gunjan, A., Hock, R., Bustin, M. & Brown, 1729  
 1666 D. T. (2000). Dynamic binding of histone H1 to 1730  
 1667 chromatin in living cells. *Nature*, **408**, 877–881. 1731
- 1668 12. Annunziato, A. T. & Seale, R. L. (1982). Maturation of 1732  
 1669 nucleosomal and nonnucleosomal components of 1733  
 1670 nascent chromatin: differential requirements for con- 1734  
 1671 current protein synthesis. *Biochemistry*, **21**, 5431–5438. 1735
- 1672 13. Annunziato, A. T., Schindler, R. K., Thomas, C. A., Jr, 1736  
 1673 & Seale, R. L. (1981). Dual nature of newly replicated 1737  
 1674 chromatin. Evidence for nucleosomal and non- 1738  
 1675 nucleosomal DNA at the site of native replication 1739  
 1676 forks. *J. Biol. Chem.* **256**, 11880–11886. 1740
- 1677 14. Bavykin, S., Srebrev, L., Banchev, T., Tsanev, R., 1741  
 1678 Zlatanova, J. & Mirzabekov, A. (1993). Histone H1 1742  
 1679 deposition and histone–DNA interactions in repli- 1743  
 1680 cating chromatin. *Proc. Natl Acad. Sci. USA*, **90**, 1744  
 1681 3918–3922. 1745
- 1682 15. Tremethick, D. J. (2007). Higher-order structures of 1746  
 1683 chromatin: the elusive 30 nm fiber. *Cell*, **128**, 651–654. 1747
- 1684 16. van Holde, K. & Zlatanova, J. (2007). Chromatin fiber 1748  
 1685 structure, where is the problem now? *Semin. Cell Dev. 1749*  
 1686 *Biol.* **18**, 651–658. 1750
- 1687 17. Finch, J. T. & Klug, A. (1976). Solenoidal model for 1751  
 1688 superstructure in chromatin. *Proc. Natl Acad. Sci. 1752*  
 1689 *USA*, **73**, 1897–1901. 1753
18. Staynov, D. Z. (1983). Possible nucleosome arrange- 1690  
 ments in the higher-order structure of chromatin. *Int. 1691*  
*J. Biol. Macromol.* **5**, 3–9. 1692
19. Williams, S. P., Athey, B. D., Muglia, L. J., Schappe, 1693  
 R. S., Gough, A. H. & Langmore, J. P. (1986). 1694  
 Chromatin fibers are left-handed double helices 1695  
 with diameter and mass per unit length that depend 1696  
 on linker length. *Biophys. J.* **49**, 233–248. 1697
20. Athey, B. D., Smith, M. F., Rankert, D. A., Williams, 1698  
 S. P. & Langmore, J. P. (1990). The diameters of 1699  
 frozen-hydrated chromatin fibers increase with 1700  
 DNA linker length: evidence in support of variable 1701  
 diameter models for chromatin. *J. Cell Biol.* **111**, 1702  
 795–806. 1703
21. Horowitz, R. A., Agard, D. A., Sedat, J. W. & 1704  
 Woodcock, C. L. (1994). The three-dimensional 1705  
 architecture of chromatin in situ: electron tomography 1706  
 reveals fibers composed of a continuously variable 1707  
 zig-zag nucleosomal ribbon. *J. Cell Biol.* **125**, 1–10. 1708
22. Dorigo, B., Schalch, T., Kulangara, A., Duda, S., 1709  
 Schroeder, R. R. & Richmond, T. J. (2004). Nucleo- 1710  
 some arrays reveal the two-start organization of the 1711  
 chromatin fiber. *Science*, **306**, 1571–1573. 1712
23. Smith, M. F., Athey, B. D., Williams, S. P. & 1713  
 Langmore, J. P. (1990). Radial density distribution 1714  
 of chromatin: evidence that chromatin fibers have 1715  
 solid centers. *J. Cell Biol.* **110**, 245–254. 1716
24. Sun, J., Zhang, Q. & Schlick, T. (2005). Electrostatic 1717  
 mechanism of nucleosomal array folding revealed by 1718  
 computer simulation. *Proc. Natl Acad. Sci. USA*, **102**, 1719  
 8180–8185. 1720
25. Stehr, R., Kepper, N., Rippe, K. & Wedemann, G. 1721  
 (2008). The effect of internucleosomal interaction on 1722  
 folding of the chromatin fiber. *Biophys. J.* **95**, 1723  
 3677–3691. 1724
26. Wong, H., Victor, J.-M. & Mozziconacci, J. (2007). An 1725  
 all-atom model of the chromatin fiber containing 1726  
 linker histones reveals a versatile structure tuned by 1727  
 the nucleosomal repeat length. *PLoS ONE*, **2**, e877. 1728
27. Rydberg, B., Holley, W. R., Mian, I. S. & Chatterjee, 1729  
 A. (1998). Chromatin conformation in living cells: 1730  
 support for a zig-zag model of the 30 nm chromatin 1731  
 fiber. *J. Mol. Biol.* **284**, 71–84. 1732
28. Routh, A., Sandin, S. & Rhodes, D. (2008). Nucleo- 1733  
 some repeat length and linker histone stoichiometry 1734  
 determine chromatin fiber structure. *Proc. Natl Acad. 1735*  
*Sci. USA*, **105**, 8872–8877. 1736
29. Davey, C. A., Sargent, D. F., Luger, K., Mäder, A. W. 1737  
 & Richmond, T. J. (2002). Solvent mediated interac- 1738  
 tions in the structure of the nucleosome core particle 1739  
 at 1.9 Å resolution. *J. Mol. Biol.* **319**, 1097–1113. 1740
30. Schalch, T., Duda, S., Sargent, D. F. & Richmond, T. J. 1741  
 (2005). X-ray structure of a tetranucleosome and its 1742  
 implications for the chromatin fibre. *Nature*, **436**, 1743  
 138–141. 1744
31. Dorigo, B., Schalch, T., Kulangara, A. & Duda, S. 1745  
 (2004). Nucleosome arrays reveal the two-start 1746  
 organization of the chromatin fiber. *Science*, **306**, 1747  
 1571–1573. 1748
32. McGhee, J. D., Nickol, J. M., Felsenfeld, G. & Rau, 1749  
 D. C. (1983). Higher order structure of chromatin: 1750  
 orientation of nucleosomes within the 30 nm 1751  
 chromatin solenoid is independent of species and 1752  
 spacer length. *Cell*, **33**, 831–841. 1753

- 1754 33. Butler, P. (1984). A defined structure of the 30 nm  
1755 chromatin fibre which accommodates different nu-  
1756 cleosomal repeat lengths. *EMBO J.* **3**, 2599–2604.
- 1757 34. Widom, J. & Klug, A. (1985). Structure of the 300 Å  
1758 chromatin filament: X-ray diffraction from oriented  
1759 samples. *Cell*, **43**, 207–213.
- 1760 35. Godde, J. S. & Widom, J. (1992). Chromatin structure  
1761 of *Schizosaccharomyces pombe*: a nucleosome repeat  
1762 length that is shorter than the chromatosomal DNA  
1763 length. *J. Mol. Biol.* **226**, 1009–1025.
- 1764 36. Huynh, V. A., Robinson, P. J. & Rhodes, D. (2005). A  
1765 method for the in vitro reconstitution of a defined  
1766 “30 nm” chromatin fibre containing stoichiometric  
1767 amounts of the linker histone. *J. Mol. Biol.* **345**,  
1768 957–968.
- 1769 37. Robinson, P. J. J., Fairall, L., Huynh, V. A. T. &  
1770 Rhodes, D. (2006). EM measurements define the  
1771 dimensions of the “30-nm” chromatin fiber: evidence  
1772 for a compact interdigitated structure. *Proc. Natl  
1773 Acad. Sci. USA*, **103**, 6506–6511.
- 1774 38. Robinson, P. J. & Rhodes, D. (2006). Structure of the  
1775 “30 nm” chromatin fibre: a key role for the linker  
1776 histone. *Curr. Opin. Struct. Biol.* **16**, 336–343.
- 1777 39. Kruithof, M., Chien, F.-T., Routh, A., Logie, C.,  
1778 Rhodes, D. & van Noort, J. (2009). Single-molecule  
1779 force spectroscopy reveals a highly compliant helical  
1780 folding for the 30-nm chromatin fiber. *Nat. Struct.  
1781 Mol. Biol.* **16**, 534–540.
- 1782 40. Aumann, F., Sühnel, J., Langowski, J. & Diekmann, S.  
1783 (2010). Rigid assembly and Monte Carlo models of  
1784 stable and unstable chromatin structures: the effect of  
1785 nucleosomal spacing. *Theor. Chem. Acc.* **125**, 217–231.
- 1786 41. Zhang, Q., Beard, D. A. & Schlick, T. (2003).  
1787 Constructing irregular surfaces to enclose macro-  
1788 molecular complexes for mesoscale modeling using  
1789 the discrete surface charge optimization (DiSCO)  
1790 algorithm. *J. Comp. Chem.* **24**, 2063–2074.
- 1791 42. Arya, G., Zhang, Q. & Schlick, T. (2006). Flexible  
1792 histone tails in a new mesoscopic oligonucleosome  
1793 model. *Biophys. J.* **91**, 133–150.
- 1794 43. Arya, G. & Schlick, T. (2006). Role of histone tails in  
1795 chromatin folding revealed by a new mesoscopic  
1796 oligonucleosome model. *Proc. Natl Acad. Sci. USA*,  
1797 **103**, 16236–16241.
- 1798 44. Arya, G. & Schlick, T. (2007). Efficient global  
1799 biopolymer sampling with end-transfer configura-  
1800 tional bias Monte Carlo. *J. Chem. Phys.* **126**, 044107.
- 1801 45. Arya, G. & Schlick, T. (2009). A tale of tails: how  
1802 histone tails mediate chromatin compaction in  
1803 different salt and linker histone environments.  
1804 *J. Phys. Chem. A*, **113**, 4045–4059.
- 1805 46. Grigoryev, S. A., Arya, G., Correll, S., Woodcock,  
1806 C. L. & Schlick, T. (2009). Evidence for hetero-  
1807 morphic chromatin fibers from analysis of nucle-  
1808 osome interactions. *Proc. Natl Acad. Sci. USA*, **106**,  
1809 13317–13322.
- 1810 47. Allison, S., Austin, R. & Hogan, M. (1989). Bending  
1811 and twisting dynamics of short linear DNAs.  
1812 Analysis of the triplet anisotropy decay of a 209  
1813 base pair fragment by Brownian simulation. *J. Chem.  
1814 Phys.* **90**, 3843–3854.
- 1815 48. Wedemann, G. & Langowski, J. (2002). Computer  
1816 simulation of the 30-nm chromatin fiber. *Biophys. J.*  
1817 **82**, 2847–2859.
- 1818 49. Bharath, M. M., Chandra, N. R. & Rao, M. R. (2003).  
1819 Molecular modeling of the chromatosome particle.  
1820 *Nucleic Acids Res.* **31**, 4264–4274.
- 1821 50. Mozziconacci, J. & Victor, J.-M. (2003). Nucleosome  
1822 gapping supports a functional structure for the 30 nm  
1823 chromatin fiber. *J. Struct. Biol.* **143**, 72–76.
- 1824 51. Korolev, N., Lyubartsev, A. P. & Nordenskiöld, L.  
1825 (2006). Computer modeling demonstrates that elec-  
1826 trostatic attraction of nucleosomal DNA is mediated  
1827 by histone tails. *Biophys. J.* **90**, 4305–4316.
- 1828 52. Mühlbacher, F., Schiessel, H. & Holm, C. (2006). Tail-  
1829 induced attraction between nucleosome core parti-  
1830 cles. *Phys. Rev. E*, **74**, 031919.
- 1831 53. Kepper, N., Foethke, D., Stehr, R., Wedemann, G. &  
1832 Rippe, K. (2008). Nucleosome geometry and inter-  
1833 nucleosomal interactions control the chromatin fiber  
1834 conformation. *Biophys. J.* **95**, 3692–3705.
- 1835 54. Voltz, K., Trylska, J., Tozzini, V., Kurkal-Siebert, V.,  
1836 Langowski, J. & Smith, J. (2008). Coarse-grained force  
1837 field for the nucleosome from self-consistent multi-  
1838 scaling. *J. Comp. Chem.* **29**, 1429–1439.
- 1839 55. Hansen, J. C., Ausio, J., Stanik, V. H. & van Holde,  
1840 K. E. (1989). Homogeneous reconstituted oligonu-  
1841 cleosomes, evidence for salt-dependent folding in the  
1842 absence of histone H1. *Biochemistry*, **28**, 9129–9136.
- 1843 56. Schlick, T. & Perišić, O. (2009). Mesoscale simulations  
1844 of two nucleosome-repeat length oligonucleosomes.  
1845 *Phys. Chem. Chem. Phys.* **11**, 10729–10737.
- 1846 57. Daban, J. R. (2000). Physical constraints in the  
1847 condensation of eukaryotic chromosomes. Local  
1848 concentration of DNA versus linear packing ratio in  
1849 higher order chromatin structures. *Biochemistry*, **39**,  
1850 3861–3866.
- 1851 58. Tse, C. & Hansen, J. C. (1997). Hybrid trypsinized  
1852 nucleosomal arrays: identification of multiple func-  
1853 tional roles of the H2A/H2B and H3/H4N-termini  
1854 in chromatin fiber compaction. *Biochemistry*, **36**,  
1855 11381–11388.
- 1856 59. Moore, S. C. & Ausió, J. (1997). Major role of the  
1857 histones H3–H4 in the folding of the chromatin fiber.  
1858 *Biochem. Biophys. Res. Commun.* **230**, 136–139.
- 1859 60. Hansen, J. C., Tse, C. & Wolffe, A. P. (1998). Structure  
1860 and function of the core histone N-termini: more than  
1861 meets the eye. *Biochemistry*, **37**, 17637–17641.
- 1862 61. Dorigo, B., Schalch, T., Bystricky, K. & Richmond,  
1863 T. J. (2003). Chromatin fiber folding: requirement for  
1864 the histone H4 N-terminal tail. *J. Mol. Biol.* **327**, 85–96.
- 1865 62. Shogren-Knaak, M., Ishii, H., Sun, J.-M., Pazin, M. J.,  
1866 Davie, J. R. & Peterson, C. L. (2006). Histone H4-K16  
1867 acetylation controls chromatin structure and protein  
1868 interactions. *Science*, **311**, 844–847.
- 1869 63. Kan, P.-Y., Lu, X., Hansen, J. C. & Hayes, J. J. (2007).  
1870 The H3 tail domain participates in multiple interac-  
1871 tions during folding and self-association of nucle-  
1872 osome arrays. *Mol. Cell. Biol.* **27**, 2084–2091.
- 1873 64. Kan, P.-Y. & Hayes, J. J. (2007). Detection of  
1874 interactions between nucleosome arrays mediated  
1875 by specific core histone tail domains. *Methods*, **41**,  
1876 278–285.
- 1877 65. Wang, X. & Hayes, J. J. (2008). Acetylation mimics  
1878 within individual core histone tail domains indi-  
1879 cate distinct roles in regulating the stability of  
1880 higher-order chromatin structure. *Mol. Cell. Biol.*  
1881 **28**, 227–236.



- 1882 66. Kan, P.-Y., Caterino, T. L. & Hayes, J. J. (2009). The  
1883 H4 tail domain participates in intra- and internucleo-  
1884 some interactions with protein and DNA during  
1885 folding and oligomerization of nucleosome arrays.  
1886 *Mol. Cell. Biol.* **29**, 538–546.
- 1887 67. Bertin, A., Durand, D., Renouard, M., Livolant, F. &  
1888 Mangenot, S. (2007). H2A and H2B tails are essential  
1889 to properly reconstitute nucleosome core particles.  
1890 *Eur. Biophys. J.* **36**, 1083–1094.
- 1891 68. Poirier, M. G., Oh, E., Tims, H. S. & Widom, J. (2009).  
1892 Dynamics and function of compact nucleosome  
1893 arrays. *Nat. Struct. Mol. Biol.* **16**, 938–944.
- 1894 69. Freidkin, I. & Katcoff, D. J. (2001). Specific distribu-  
1895 tion of the *Saccharomyces cerevisiae* linker histone  
1896 homolog HHO1p in the chromatin. *Nucleic Acids Res.*  
1897 **29**, 4043–4051.
- 1898 70. Shen, X., Yu, L., Weir, J. W. & Gorovsky, M. A. (1995).  
1899 Linker histones are not essential and affect chromatin  
1900 condensation in vivo. *Cell*, **82**, 47–56.
- 1901 71. Shen, X. & Gorovsky, M. (1996). Linker histone H1  
1902 regulates specific gene expression but not global  
1903 transcription in vivo. *Cell*, **86**, 475–483.
- 1904 72. Chambers, S. A. M., Vaughn, J. P. & Ramsay-Shaw,  
1905 B. (1983). Shortest nucleosomal repeat lengths during  
1906 sea urchin development are found in two-cell  
1907 embryos. *Biochemistry*, **22**, 5626–5631.
- 1908 73. D'Anna, J. A. & Tobey, R. A. (1989). Changes in  
1909 nucleosome repeat lengths precede replication in the  
1910 early replicating metallothionein II gene region of  
1911 cells synchronized in early S phase. *Biochemistry*, **28**,  
1912 2895–2902.
- 1913 74. Beard, D. A. & Schlick, T. (2001). Computational  
1914 modeling predicts the structure and dynamics of  
1915 chromatin fiber. *Structure*, **9**, 105–114.
- 1916 75. Beard, D. A. & Schlick, T. (2001). Modeling salt-  
1917 mediated electrostatics of macromolecules: the discrete  
1918 surface charge optimization algorithm and its appli-  
1919 cation to the nucleosome. *Biopolymers*, **58**, 106–115.
- 1920 76. Heath, P. J., Gebe, J. A., Allison, S. A. & Schurr, J. M.  
1921 (1996). Comparison of analytical theory with Brown-  
1922 nian dynamics simulations for small linear and  
1923 circular DNAs. *Macromolecules*, **29**, 3583–3596.
- 1924 77. Schlick, T. & Fogelson, A. (1992). TNPACK—a  
1925 truncated Newton minimization package for large-  
1926 scale problems: I. Algorithm and usage. *ACM Trans.*  
1927 *Math. Softw.* **18**, 46–70.
- 1928 78. Schlick, T. & Fogelson, A. (1992). TNPACK—a  
1929 truncated Newton minimization package for large-  
1930 scale problems: II. Implementation examples. *ACM*  
1931 *Trans. Math. Softw.* **18**, 71–111.
- 1932 79. Xie, D. X. & Schlick, T. (1999). Efficient implementa-  
1933 tion of the truncated-Newton algorithm for large-  
1934 scale chemistry applications. *SIAM J. Optim.* **10**,  
1935 132–154.
- 1936 80. Gilson, M. K., Sharp, K. A. & Honig, B. H. (1988).  
1937 Calculating the electrostatic potential of molecules in  
1938 solution: method and error assessment. *J. Comput.*  
1939 *Chem.* **9**, 327–335.
- 1940 81. Sharp, K. A. & Honig, B. (1990). Electrostatic  
1941 interactions in macromolecules: theory and applica-  
1942 tions. *Annu. Rev. Biophys. Biophys. Chem.* **19**, 301–332.
- 1943 82. Sharp, K. A. & Honig, B. (1990). Calculating total  
1944 electrostatic energies with the nonlinear Poisson–  
1945 Boltzmann equation. *J. Phys. Chem.* **94**, 7684–7692.
83. Connolly, M. L. (1983). Solvent-accessible surfaces of 1946  
1947 proteins and nucleic acids. *Science*, **221**, 709–713.
84. Cornell, W. D., Cieplak, P., Bayly, C. I., Gould, I. R., 1948  
1949 Merz, K. M., Ferguson, D. M. *et al.* (1995). A second  
1950 generation force field for the simulation of proteins,  
1951 nucleic acids, and organic molecules. *J. Am. Chem.*  
1952 *Soc.* **117**, 5179–5197.
85. Stigter, D. (1977). Interactions of highly charged 1953  
1954 colloidal cylinders with applications to double-  
1955 stranded DNA. *Biopolymers*, **16**, 1435–1448.
86. Drew, H. R. & Travers, A. A. (1985). DNA bending 1956  
1957 and its relation to nucleosome positioning. *J. Mol.*  
1958 *Biol.* **186**, 773–790.
87. Deng, J., Pan, B. & Sundaralingam, M. (2003). 1959  
1960 Structure of d(ITITACAC) complexed with distamy-  
1961 cin at 1.6 Å resolution. *Acta Crystallogr. Sect. D: Biol.*  
1962 *Crystallogr.* **59**, 2342–2344.
88. Q. Zhang. (2005). Mesoscopic, microscopic, and 1963  
1964 macroscopic modeling of protein/DNA complexes.  
1965 PhD thesis, New York University, New York.
89. Bharath, M. M., Chandra, N. R. & Rao, M. R. (2002). 1966  
1967 Predictions of an HMg-box fold in the C-terminal  
1968 domain of histone H1: insight into its role in DNA  
1969 condensation. *Proteins*, **49**, 71–81.
90. Sheng, S., Czajkowsky, D. M. & Shao, Z. (2006). 1970  
1971 Localization of linker histone in chromatosomes by  
1972 cryo-atomic force microscopy. *Biophys. J.* **91**, L35–L37.
91. Baumann, C. G., Smith, S. B., Bloomfield, V. A. & 1973  
1974 Bustamante, C. (1997). Ionic effects on the elasticity of  
1975 single DNA molecules. *Proc. Natl Acad. Sci. USA*, **94**,  
1976 6185–6190.
92. Rouzina, I. & Bloomfield, V. A. (1998). DNA bending 1977  
1978 by small, mobile multivalent cations. *Biophys. J.* **74**,  
1979 3152–3164.
93. H. H. Gan & T. Schlick. (2010). Chromatin ionic 1980  
1981 atmosphere analyzed by a mesoscale electrostatic  
1982 approach. Submitted.
94. Frenkel, D., Mooij, G. C. A. M. & Smit, B. (1992). 1983  
1984 Novel scheme to study structural and thermal  
1985 properties of continuously deformable molecules.  
1986 *J. Phys. Condens. Matter*, **4**, 3053–3076.
95. de Pablo, J. J., Laso, M. & Suter, U. W. (1992). 1987  
1988 Simulation of polyethylene above and below the  
1989 melting point. *J. Chem. Phys.* **96**, 2395–2403.
96. Rosenbluth, M. N. & Rosenbluth, A. W. (1955). 1990  
1991 Monte Carlo calculation of the average extension of  
1992 molecular chains. *J. Chem. Phys.* **23**, 356–359.
97. Williams, S. P. & Langmore, J. P. (1991). Small angle 1993  
1994 X-ray scattering of chromatin. Radius and mass per  
1995 unit length depend on linker length. *Biophys. J.* **59**,  
1996 606–618.
98. Gerchman, S. E. & Ramakrishnan, V. (1987). Chro- 1997  
1998 matin higher-order structure studied by neutron  
1999 scattering and scanning transmission electron mi-  
2000 croscopy. *Proc. Natl Acad. Sci. USA*, **84**, 7802–7806.
99. Yao, J., Lowary, P. T. & Widom, J. (1990). Direct 2001  
2002 detection of linker DNA bending in defined-length  
2003 oligomers of chromatin. *Proc. Natl Acad. Sci. USA*, **87**,  
2004 7603–7607.
100. Yao, J., Lowary, P. & Widom, J. (1991). Linker DNA 2005  
2006 bending induced by the core histones of chromatin.  
2007 *Biochemistry*, **30**, 8408–8414.
101. Bednar, J., Horowitz, R. A., Dubochet, J. & 2008  
2009 Woodcock, C. (1995). Chromatin conformation and

- 2010 salt-induced compaction: three-dimensional structural information from cryoelectron microscopy. *J. Cell Biol.* **131**, 1365–1376.
- 2011
- 2012
- 2013 102. Bertin, A., Leforestier, A., Durand, D. & Livolant, F. (2004). Role of histone tails in the conformation and interactions of nucleosome core particles. *Biochemistry*, **43**, 4773–4780.
- 2014
- 2015
- 2016
- 2017 103. Leuba, S. H., Yang, G., Robert, C., Samori, B., van Holde, K., Zlatanova, J. & Bustamante, C. (1994). Three-dimensional structure of extended chromatin fibers as revealed by tapping-mode scanning force microscopy. *Proc. Natl Acad. Sci. USA*, **91**, 11621–11625.
- 2018
- 2019
- 2020
- 2021
- 2022
- 2023 104. Toth, K., Brun, N. & Langowski, J. (2006). Chromatin compaction at the mononucleosome level. *Biochemistry*, **45**, 1591–1598.
- 2024
- 2025
- 2026 105. van Holde, K. & Zlatanova, J. (1996). What determines the folding of the chromatin fiber? *Proc. Natl Acad. Sci. USA*, **93**, 10548–10555.
- 2027
- 2028
- 2029 106. Kepert, J. F., Toth, K. F., Caudron, M., Mucke, N., Langowski, J. & Rippe, K. (2003). Conformation of reconstituted mononucleosomes and effect of linker histone H1 binding studied by scanning force microscopy. *Biophys. J.* **85**, 4012–4022.
- 2030
- 2031
- 2032
- 2033
- 2034 107. Bloomfield, V., Dalton, W. O. & van Holde, K. E. (1967). Frictional coefficients of multisubunit structures. I. Theory. *Biopolymers*, **5**, 135–148.
- 2035
- 2036
- 2037 108. Kirkwood, J. G. (1954). The general theory of irreversible processes in solutions of macromolecules. *J. Polym. Sci.* **12**, 1–14.
- 2038
- 2039
- 2040 109. Garcia-Ramirez, M., Dong, F. & Ausio, J. (1992). Role of the histone “tails” in the folding of oligonucleosomes depleted of histone H1. *J. Biol. Chem.* **267**, 19587–19595.
- 2041
- 2042
- 2043
- 2044 110. Garcia de la Torre, J., Navarro, S., Lopez Martinez, M. C., Diazand, F. G. & Lopez Cascales, J. J. (1994). HYDRO: a computer program for the prediction of hydrodynamic properties of macromolecules. *Biophys. J.* **67**, 530–531.
- 2045
- 2046
- 2047
- 2048
- 2049 111. Morris, N. R. (1976). Nucleosome structure in *Aspergillus nidulans*. *Cell*, **8**, 357–363.
- 2050
- 2051 112. Pearson, E. C., Bates, D. L., Prospero, T. D. & Thomas, J. O. (1984). Neuronal nuclei and glial nuclei from mammalian cerebral cortex. Nucleosome repeat lengths, DNA contents and H1 contents. *Eur. J. Biochem.* **144**, 353–360.
- 2052
- 2053
- 2054
- 2055
- 2056 113. Downs, J. A., Kosmidou, E., Morgan, A. & Jackson, S. P. (2003). Suppression of homologous recombination by the *Saccharomyces cerevisiae* linker histone. *Mol. Cell*, **11**, 1685–1692.
- 2057
- 2058
- 2059
- 2060 114. Noll, M. (1976). Differences and similarities in chromatin structure of *Neurospora crassa* and higher eucaryotes. *Cell*, **8**, 349–355.
- 2061
- 2062
- 2063 115. Fan, Y., Nikitina, T., Morin-Kensicki, E. M., Zhao, J., Magnuson, T. R., Woodcock, C. L. & Skoultchi, A. I. (2003). H1 linker histones are essential for mouse development and affect nucleosome spacing in vivo. *Mol. Cell. Biol.* **23**, 4559–4572.
- 2064
- 2065
- 2066
- 2067
- 2068 116. Stalder, J. & Braun, R. (1978). Chromatin structure of *Physarum polycephalum* plasmodia and amoebae. *FEBS Lett.* **90**, 223–227.
- 2069
- 2070
- 2071 117. Bates, D. L. & Thomas, J. O. (1981). Histones H1 and H5: one or two molecules per nucleosome? *Nucleic Acids Res.* **25**, 5883–5894.
- 2072
- 2073